DTIC FILE COPY

②

REPORT DOCUMENTATION PAGE

Form Approved
OMB No. 0704-0188

AD-A214 923

1. AGENCY USE ONLY (Leave blank)	2. REPORT DATE	3. REPORT TYPE AND DATES COVERED
	Apr 79	Final 1 Jan 74- 31 Oct 78

4. TITLE AND SUBTITLE
FLUID MECHANICAL REFRACTING GAS PRISM AND AERODYAMICS OF
E-BEAM SUSTANINED DISCHARGE IN SUPERSONIC FLOW, 80th
APPLICABLE TO LASER TECHNOLOGY

5. FUNDING NUMBERS

61102F
2307/A3

6. AUTHOR(S)

D.W. BOGDANOFF   W.H. CHRISTIANSEN

7. PERFORMING ORGANIZATION NAME(S) AND ADDRESS(ES)

UNIVERSITY OF WASHINGTON
AEROSPACE & ENERGETICS RESEARCH PROGRAM
SEATTLE, WASHINGTON 98195

8. PERFORMING ORGANIZATION REPORT NUMBER

AFOSR-TR- 89-1427

9. SPONSORING/MONITORING AGENCY NAME(S) AND ADDRESS(ES)

AFOSR
BLDG 410
BAFB DC 20332-6448

10. SPONSORING/MONITORING AGENCY REPORT NUMBER

AFOSR 74-2650

11. SUPPLEMENTARY NOTES

12a. DISTRIBUTION/AVAILABILITY STATEMENT

12b. DISTRIBUTION CODE

13. ABSTRACT (Maximum 200 words)

DTIC
ELECTE
NOV 29 1989
S B D

14. SUBJECT TERMS			15. NUMBER OF PAGES
			63
			16. PRICE CODE

17. SECURITY CLASSIFICATION OF REPORT	18. SECURITY CLASSIFICATION OF THIS PAGE	19. SECURITY CLASSIFICATION OF ABSTRACT	20. LIMITATION OF ABSTRACT
UNCLASSIFIED	UNCLASSIFIED		

NSN 7540-01-280-5500

89 11 27 086

Standard Form 298 (890104 Draft)
Prescribed by ANSI Std. 239-18
298-01

FLUID MECHANICAL REFRACTING GAS PRISM AND AERODYNAMICS

OF E-BEAM SUSTAINED DISCHARGE IN SUPERSONIC FLOW,

BOTH APPLICABLE TO LASER TECHNOLOGY

AFOSR #74-2650

Final Annual Report

1 January 1974 - 31 October 1978

D.W. Bogdanoff

W.H. Christiansen

Aerospace & Energetics Research Program

University of Washington

Seattle, Washington

April 1979

Final Annual Report

FLUID MECHANICAL REFRACTING GAS PRISM AND AERODYNAMICS
OF E-BEAM SUSTAINED DISCHARGE IN SUPERSONIC FLOW,
BOTH APPLICABLE TO LASER TECHNOLOGY

I. INTRODUCTION

In many high power laser systems, the interaction of either electro-magnetic radiation or an electric discharge with a flow system has proved an important phenomenon. For example, knowledge of the interaction of laser radiation and flow is required to understand the performance of aerodynamic windows and the nonlinear effects of thermal blooming, The last phenomenon involves significant effects caused by small energy losses of the beam. The small losses usually associated with simple refraction of light in gases may be useful and have motivated us to develop and study a unique fluid mechanical device for possible manipulation and storage of laser radiation.

In the work performed to date, we have shown that a low power beam of light can be deflected continuously through large angles along a curved path using the flow from a convergent-divergent nozzle sector whose throat lies on an arc of a circle. The flow devices that have been built and studied, based on this concept, have been dubbed Venus machines because of the similarity to the optical conditions predicted to exist in the atmosphere of Venus. The nozzle sectors as nominally selected included angles of 30°, 90°, and 180° and have been studied both theoretically and experimentally. Further, a visible laser beam on the order of a megawatt of power has been deflected

through a 90° turn. In all these devices it has been clearly demonstrated that a well-defined region exists in the flow wherein light rays are trapped in near circular paths. The effect is similar to an optical wave guide lying on a circular path.

New and more accurate transmission data is presented in this report wherein transmission measurements in excess of 99.5% are detailed. This data permits detailed analysis of the light well and a more accurate assessment of the optimum operating conditions of the Venus Machine. Only studies carried out during the 1978 year are reported herein. Previous accrual reports may be used to cover the earlier period of the grant.

An electron-beam sustained electric discharge laser producing either pulsed or continuous power laser radiation from a supersonic gas flow is a promising approach for high-power laser development. The utility of the supersonic expansion as a means for achieving low gas temperatures required for efficient laser performance is known. The electric glow discharge in supersonic flow presents a fascinating array of complex aerodynamic problems that are very different from those associated with gasdynamic and chemical lasers. For example, supersaturated mixtures and condensation may be a problem if cyrogenic temperatures are used. At these low temperatures, too, any heat addition to the flowing gas stream creates large relative changes in temperature, affecting the performance of the laser. In addition, there are large losses in total pressure of the system that may affect the ability to completely diffuse the flow to the atmosphere. We have studied the fundamental mechanisms of the interaction of electrical discharges of the

glow type and the fluid mechanics as normally found in electric discharge lasers in an effort to improve their performance capability. Basic information on these devices is being obtained via small-scale experiments using the available facilities at the University of Washington. This report gives a summary of the progress made to date on the aerodynamic aspects of this program.

II. SUMMARY OF PROGRESS

As previously mentioned, we are studying fluid mechanical optics (in the form of a gasdynamic light guide) and aerodynamics of high power glow discharges.

A. Aerodynamics of E-Beam Sustained Discharges

(1) The Supersonic Flow Facility and Discharge Apparatus. At the University of Washington we have a flow facility and power supplies that can simulate in a satisfactory way the discharge characteristics of a large scale laser discharge facility. This facility was completed during 1978. A short description of the facility and its characteristics is given in this section. Basically, we simulate the flow and discharge characteristics of a large scale electric laser, using a combination of long duration pulsed flow and electric discharges. Fig. 1 is a drawing of the facility showing some of the important elements, and Fig. 2 is a photograph of the setup. A 6" diameter Ludwieg tube provides the flow of gas required for the discharge. It is capable of storing gas at up to 300 psia. The gas is expanded through a conventional 2-D nozzle system which at present gives rise to a flow cross section of 4 cm x 20 cm. A M = 3.2 nozzle can be seen in Fig. 2.

The duration and quality of the flow have been examined, using pressure gauges and double pulse laser holographic interferometry. After an initial transient of 2 msec duration, the pressure in the plenum chamber becomes nearly constant (except for noise) giving a testing time in excess of 8 msec. Additional lengths of tube are available should they be necessary to increase the flow duration. The Mach number of the flow was measured and found to be M = 3.2 ± 3% in agreement with calculations. Fig. 3 shows the photograph from which this was measured.

The discharge is located in the supersonic channel and is stabilized by an e-beam. This e-beam is produced by a 6" diameter plasma diode and capable of being operated at up to 150 kV. We have operated the system at voltages as high as 135 kV in tests. The duration of the discharge and e-beam current can be easily controlled. Time duration from 10 μsec to many times the transit time of a particle through the discharge can be obtained. Our design aim has been used to supply e-beam current through a duration in excess of six times this transit time scale (transit time order of 50 μsec) with a corresponding voltage drop of no more than 10% on the diode. At lower current densities longer time scales are possible, perhaps considerably in excess of 1 msec. A typical e-beam current and voltage trace is given in Fig. 4. Both the input current to the diode and e-beam output are shown. As can be seen, the output is only a fraction of the input current, typical of plasma diodes. Nevertheless, current densities from 1 ma/cm^2 to 30 ma/cm^2 have been measured from the diode without foil failure. These current densities are somewhat higher than contemplated CW or high repetition rate systems. We are thus

able to provide higher electron densities and therefore higher sustainer current to pump the system more rapidly. The gas energy content can be scaled properly, of course, allowing a shorter discharge in the flow direction. The higher current densities of the plasma diode,[1] in comparison to the thermionic gun,[2] alleviate much of the problem of dissociative attachment caused by low concentration (ppm) impurities that plague so many of the low current devices. A high energy capacitor bank was built for the sustainer. We are able to draw currents in excess of 40 amp. for the testing time with a minimal (10%) voltage drop. The characteristics of the e-beam sustainer system are shown in Fig. 5. Delay circuits make it possible to independently turn on and off both e-beam and sustainer currents. In this way we can choose times for the most uniform conditions. At the highest e-beam current levels, power densities in the discharge are in excess of 10^7 w/liter-amagat.

(2) <u>Measurements on the Discharge</u>. An extensive series of measurements of the effect of the discharge on the flow field were taken using a laser holographic technique. These measurements involve a no-flow case as well as the supersonic flow case.

Early interferograms in the static case showed severe heating of the gas near the electrode edges. This is a result of high field strength at the edges of the finite electrodes and the concentration of current there as well. We have also clearly observed extensive cathode fall heating and the cathode shock wave. Of particular interest to us is the rather large region near the cathode in which a non-uniform density appears. This density field is probably

due to heat diffusion phenomena, but it is very thick for the time scale
of the study. We are presently continuing to investigate this effect as
it may be important and useful in helping to evaluate phenomenon in the
flowing case.

Measurements have also shown the effects of discharge heating on the
boundary layer in supersonic flow. The effects of cathode fall results in
a thickening of the boundary layer and a standing oblique wave emanates from
the leading edge of the cathode. A complete discussion of these results is
contained in a recently completed Ph.D. thesis by E. Margalith entitled
"The Interaction Between E-Beam Sustained Discharge and Supersonic Flow."
A copy of the abstract of this thesis is attached for the reader's convenience
as Appendix A.

Some of the results of this work on the cathode phenomenon were presented
at the 31st Gaseous Electronics Conference held in Buffalo. The abstract of
this talk is given in Appendix B. The most complete version of this work
will be presented at the 12th International Shock Tube Symposium in Israel.
The extended abstract giving the essential features of the work is shown in
Appendix C.

B. Fluid Mechanical Optics

The small losses usually associated with simple refraction of light in
gases have motivated us to develop and study a unique fluid mechanical device
for possible manipulation and storage of laser radiation. The refractive
index gradients in the gas flow in a convergent-divergent nozzle sector whose
throat lies in the arc of a circle can create, in the neighborhood of the

throat, a region capable of trapping and guiding light. Such a device, with a deflection angle of 90° and a throat radius of 7.6 cm, was constructed and extensive measurements were taken. The working gas was nitrogen at supply pressures of 30 to 100 atm. The shape, structure and transmission characteristics of the light guiding region were investigated for a variety of nozzle operating conditions and light injection conditions. An experimental-theoretical model of the light guiding region was constructed which yielded a consistent correlation of the data. Under optimum operating conditions, the transmission of the device was measured to be greater than 99.5%. The optical quality of this (prototype) light guide was poor; however, there appears to be no reason why gasdynamic light guides of much higher quality cannot be constructed. A paper detailing these measurements is being submitted to the archival literature. The preliminary version of this work is given in Appendix D and very well describes our progress in the low power region of the Venus machine.

In the work performed to date, we have shown additionally that a beam of light can be deflected continuously through large angles along a curved path using the flow from a convergent-divergent nozzle sector whose throat lies on an arc of a circle at powers on the order of a megawatt with good transmission.

The success of these devices has led to the design of a 360° machine which will bend light in closed circular paths. The details of this device are similar to those of the 90° device swept out into a full circle. It also has a 7.6 cm radius and a 0.4 mm nozzle slit height. A large diameter

tube and valve connects it to the same pressure reservoir being used for the 90° machine. An extensive nozzle design effort was undertaken to ensure the low noise (i.e., low turbulence) flow having laminar boundary layers in the transonic region of the light well. The device itself has been constructed although as yet not tested during the grant period.

REFERENCES

1. B.B. O'Brien, Jr., Appl. Phys. Letters, 22, 503, 1973.

2. J.E. Thompson, B.B. O'Brien, C.G. Parazzoli, W.B. Lacina, "Supersonic Flow Electron Beam Stabilized CO Electric Discharge Laser," presented at 28th Ann. Gaseous Electron Conf., Rolla, Missouri, 1975.
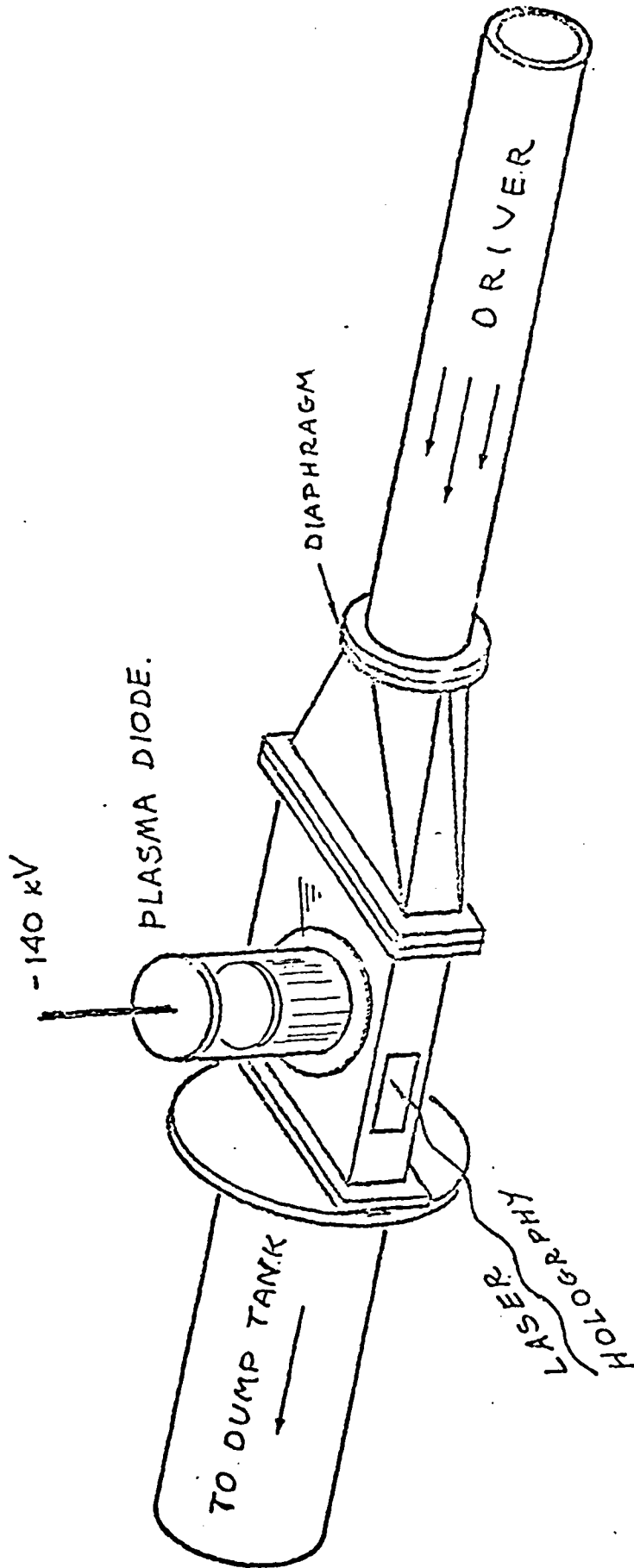
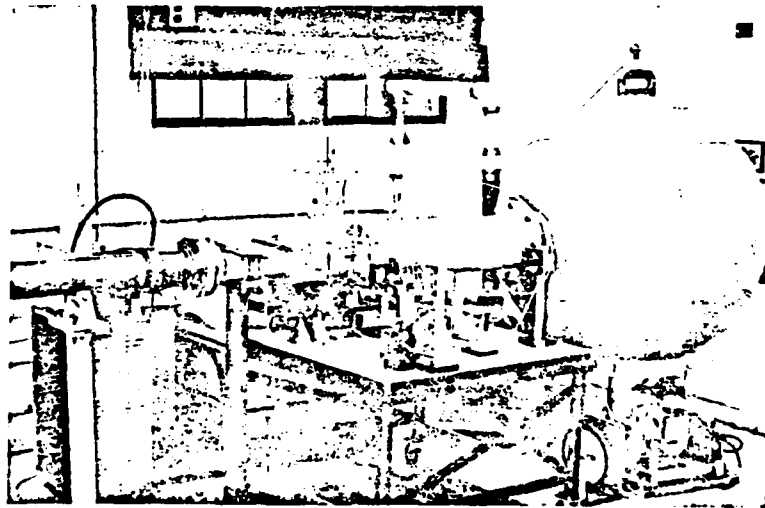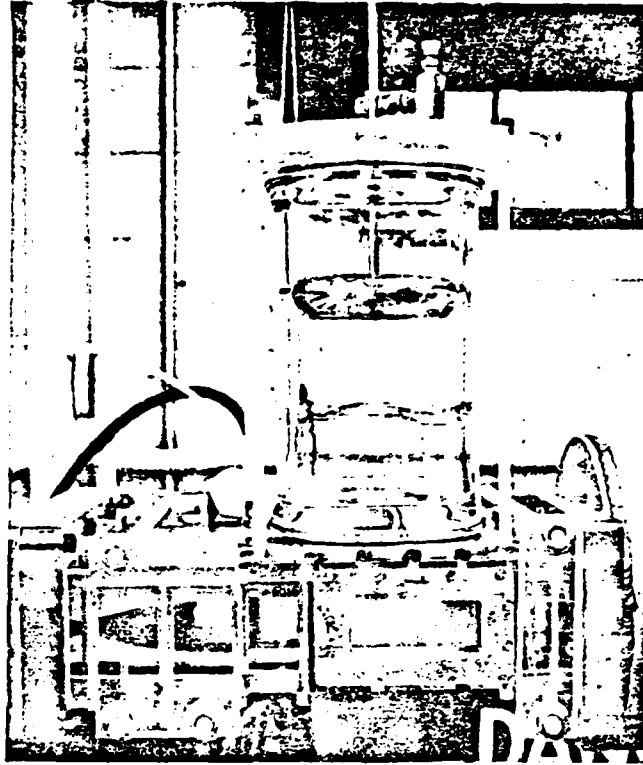Fig. 1. Schematic of Discharge/Flow Facility.

Fig. 2. Photographs of the discharge/flow facility

Boundary
Layer

Scale 5:1
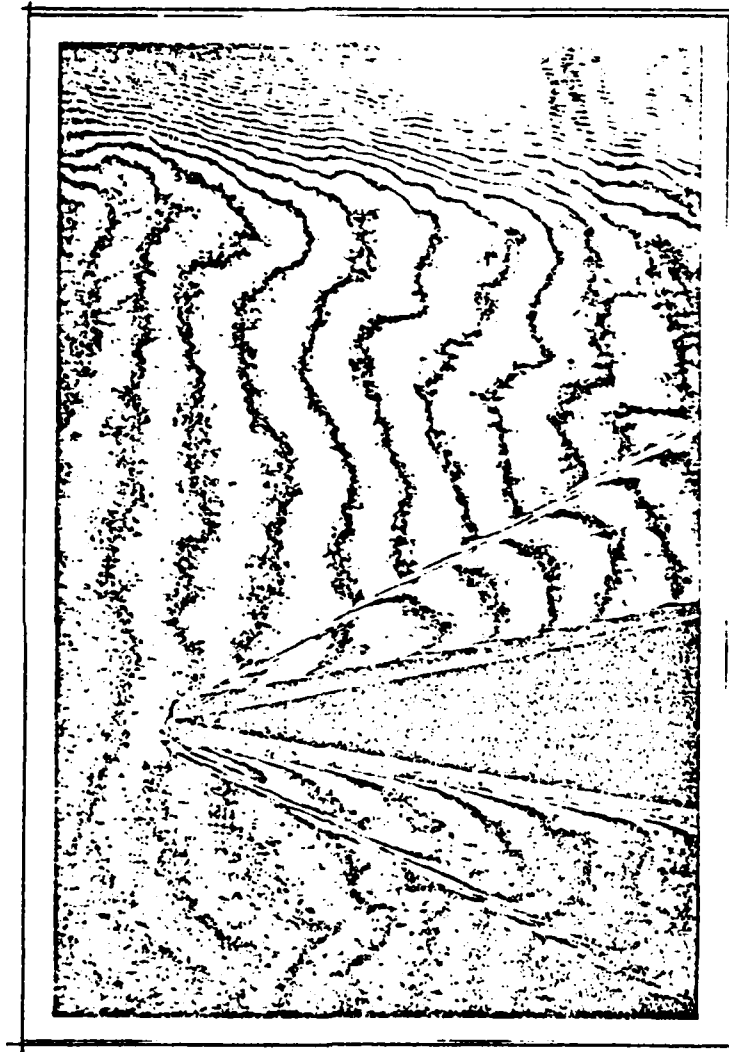
Fig. 3.   Oblique shock on 2-D wedge

V & Iout

In

P = 25µ He
V = 50 kV/div
Iout = 0.1 A/div
Iin = 5 A/div
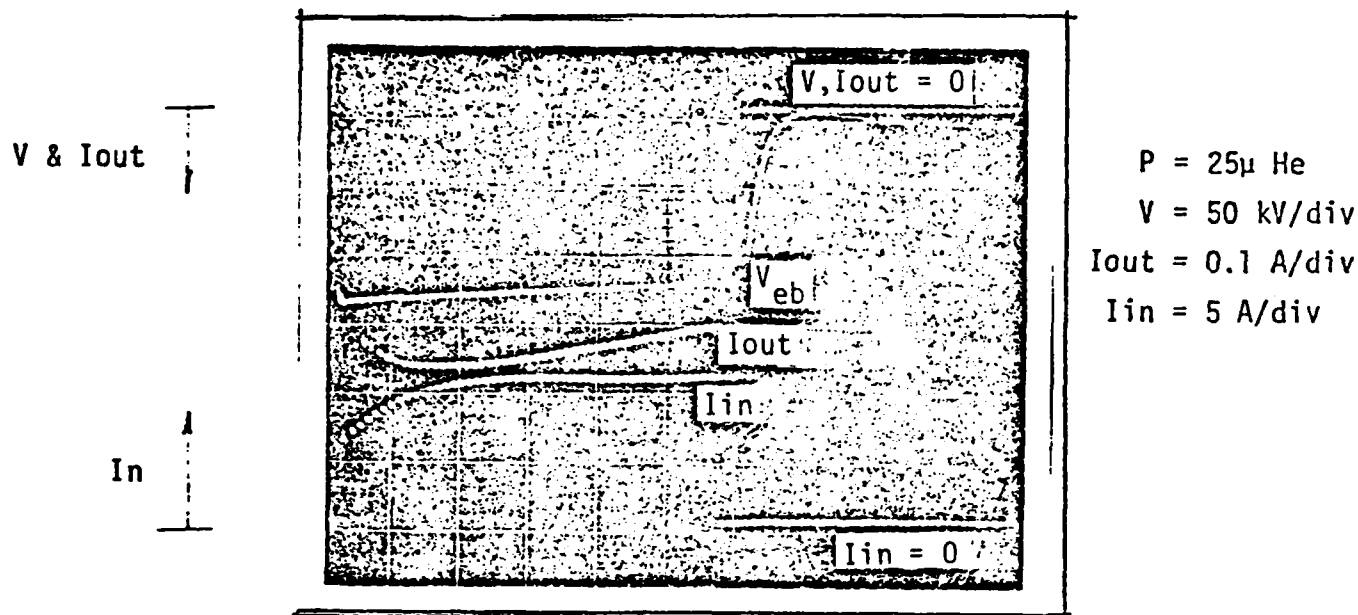
Fig. 4.   E-Beam Voltage & Current Traces
          t = 50µs/div

V_s & I_s

Iin_{eb}

V_s = 500 V/div
I_s = 100 A/div
Iin_{eb} = 5 A/div
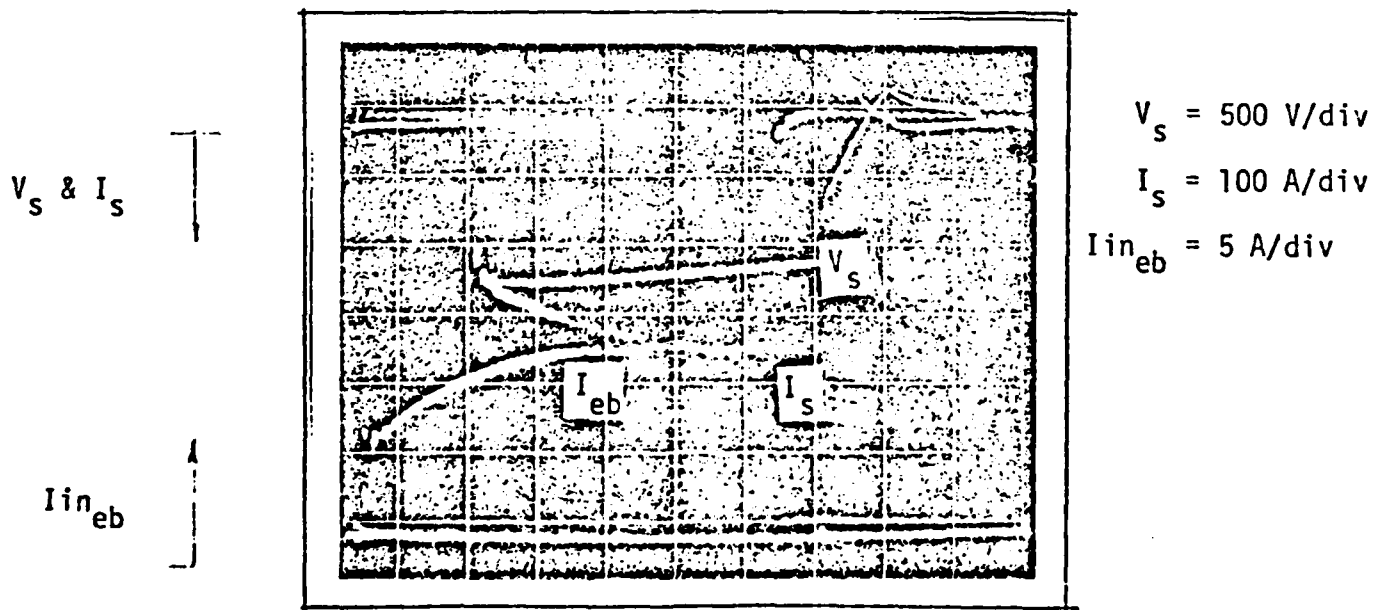
Fig. 5.   Sustainer Voltage-current traces
          t = 50µs/div

APPENDIX A

THE INTERACTION BETWEEN E-BEAM SUSTAINED

DISCHARGE AND SUPERSONIC FLOW

by

Eliyahu Margalith

A dissertation submitted in partial fulfillment
of the requirements for the degree of

Doctor of Philosophy

University of Washington

1978

Approved by _____
                    (Chairperson of Supervisory Committee)

Program Authorized
to Offer Degree _____

Date _____

University of Washington

Abstract

THE INTERACTION BETWEEN E-BEAM SUSTAINED DISCHARGE AND SUPERSONIC FLOW

by Eliyahu Margalith

Chairperson of the Supervisory Committee: Prof. W. H. Christiansen
Department of Aeronautics
and Astronautics

Results from extensive experiments in a small scale e-beam sustained electrical discharge in static gas and supersonic flow are presented. A plasma-diode e-beam gun rather than a hot-cathode gun is used as the external ionization source. It operates at current densities of 10 to 20 mA/cm^3 for several hundred microseconds. The resulting sustainer input power is increased by more than a factor of 3 over previously reported similar experiments. Supersonic flow at M = 3.2 is obtained in the test section as the gas expands from a pressurized Ludwieg tube through a contoured nozzle.

The transition to arc in static discharges is observed and compared to discharge breakdown in the flow. A difference in the performance limits of the two cases is shown and discussed.

Density disturbances, resulting from the heat release in the cathode fall are examined and related to variations in the flow boundary layer on the cathode side. The time required to reach steady state is determined by monitoring the static pressure variation during the discharge. The volumetric heating of the flow by the discharge is found to be less important than the disturbances within the boundary layer for the observed discharge instability, and the measured increase

in pressure. By removing the cathode from the existing boundary layer into the core flow, the power loading per unit volume is proved to increase by a factor of two.

APPENDIX B

THIRTY-FIRST ANNUAL GASEOUS ELECTRONICS CONFERENCE

17-20 October 1978

Buffalo, New York

PLEASE TYPE NAME & ADDRESS

Dr. W.H. Christiansen
Aero. & Energetics Research
Program, FL-10
University of Washington
Seattle, WA 98195

Observations of Density Disturbances in the Cathode Region of Electron-Beam Sustained Discharges-E. MARGALITH and W.H. CHRISTIANSEN, Univ. of Washington*--A plasma diode e-beam gun is used as an external ionization source in a sustained discharge. Power densities in excess of 200 w/cm^3 were obtained in N_2 at densities from 0.2 to 0.4 amagat for pulse lengths on the order of 200 μsec. Using holographic interferometry, the density in the vicinity of the cathode is observed. In addition to the density disturbance normally associated with the cathode shock, density variations of more than 50% are observed at the cathode vicinity following the initiation of the discharge. A characteristic propagation rate of the disturbance and related gas velocity are examined. The layer thickness reaches 5 mm to 10 mm in 100 μs depending on the discharge conditions and the gas pressure. The velocity varies in the range of 10 to 20 m/s away from the cathode and is found to be related to the ratio of the discharge current to the gas pressure. Enhanced diffusion, which is a result of nonuniform heating at the cathode, is suggested to explain the observed phenomenon. Good agreement is obtained with theoretical calculations when a diffusivity two orders of magnitude larger than the gas kinetics value is introduced.
*Supported by AFOSR Grant 74-2650.

APPENDIX C

INTERACTIONS BETWEEN AN E-BEAM SUSTAINED
DISCHARGE AND SUPERSONIC FLOW

E. Margalith and Walter H. Christiansen
University of Washington
Seattle, Washington

High pressure, large volume glow discharges have become an important topic in recent years due to the development of high power electric lasers. Supersonic flows are often used in the discharge region of these lasers to provide cyrogenic temperatures for operation and to remove waste heat (1). The interaction of the discharge and flow gives rise to some unusual problems which limit the performance of the laser and which have not yet been adequately investigated. Two problem areas have been studied experimentally in order to understand better the characteristics of discharges in flows. These are the disturbances produced by cathode phenomena in the discharge and early glow to arc transition as modified by the supersonic flow.

A small scale experiment was designed and built to simulate a continuous e-beam controlled discharge in steady supersonic flow. Quasi-steady flow is provided by a Ludwieg tube for approximately 10 ms. The gas is expanded to M = 3.2 via a contoured nozzle to temperatures and pressures on the order of 80°K and 100 Torr, respectively. The plasma-diode electron-beam gun (2) is adopted and used for the first time in a supersonic system because its current density emission is more than an order of magnitude greater than that of a thermionic gun. It can operate for several hundred microseconds as required

to simulate continuously operated systems. The high current density results in high power loading in the sustained discharge, enabling the present small scale experiment to simulate the interaction between flow and discharge of physically larger systems. The flow test section is 4 cm in height and 22 cm wide with the electrode spacing equal to the test section height. The discharge dimensions are 4 cm in the flow direction and 14 cm transverse to it, thus giving a 4 cm insulating region on each side of the discharge to prevent boundary layer shorting (1).

In order to determine the effect of flow on the transition from glow to arc, the characteristics of discharges without an external flow were observed and compared to discharges with flow. The current-voltage traces are nearly the same with and without flow if the free stream density equals that density in the static tests. THe transition to arc in static discharges was also observed and compared to discharge breakdown in flow. A correlation was found between the elapsed time (from the initiation of the discharge until the glow to arc transition) to the energy per particle deposited in the gas prior to the arc. This energy is considerably lower in the flowing case based on the free stream conditions than that under similar static conditions. It was found that the transition to arc in flow is best correlated to the static case using the gas density at the wall (within the boundary layer) whereas the current-voltage characteristics are controlled by the free stream conditions. This suggests the idea that boundary phenomena are a cause of the transition in flow.

Density disturbances, resulting from the heat release in the cathode fall, were carefully observed in the static experiments using interferometry and

were related to variations in the flow boundary layer on the cathode side. The acoustic wave originating at the cathode at the initiation of the discharge has been previously investigated by others (3,4) for different conditions; however, the thick thermal layer which follows the wave was omitted from their discussions. This layer was examined carefully in the present research. Density profiles for different discharge conditions were observed via laser holographic interferometry at various times, and the growth rate of the layer is measured.

Observation of the density variations at the cathode following the initiation of the discharge for a no flow case are presented in Fig. 1. The sensitivity, $\Delta\rho/\rho_\infty$ = 4.2% per fringe, is based on the cathode width of 14 cm. In all these experiments, the e-beam current was 14 A at 110 kV (a current density of 15 mA/cm^2). At a sustainer voltage of 3 kV, the resulting sustainer current was nearly constant at 260 A. The output of a photodiode monitoring the light from the laser interferometer is separately recorded, in order to determine the time at which the hologram is taken. The times indicated in Fig. 1 are measured from the initiation of the sustainer discharge.

The acoustic wave which propagates away from the cathode is seen clearly in the first two pictures labeled a and b. The source of this wave is the density disturbance associated with a thermal boundary layer due to the cathode fall heating. (Very little disturbance and no wave are seen at the anode side of the discharge.) While definitely a constant pressure disturbance, the growing thickness of the layer at the cathode cannot be accounted for by gas kinetic values of the diffusivity. In fact, the gas kinetic diffusivity is from two to three orders of magnitude too small to explain the thickness of the layer.

Photographs of the cathode surface taken during 20 μsec duration discharge pulses are shown in Fig. 2. These photographs show a large non-uniformity in illumination over the surface, thus implying a non-uniform current distribution and heat release at the cathode surface. From these pictures and the inter- ferograms, a one-dimensional model is proposed where the local heating gives rise to small scale flow with an apparent heat conductivity orders of magnitude greater than the gas kinetic value. The observed density variation is then a result of heat transport by a process of convectively enhanced diffusion. Good correlation between calculated density profiles and the measured ones are obtained from this model.

The results obtained in static experiments can be used to help explain the interaction between the flow boundary layer and the discharge. The contri- bution of the cathode phenomena to the boundary layer's growth rate can be separated experimentally from that due to volumetric heat addition. The effect of the cathode on the boundary layer is well shown in Fig. 3. A flat plate having the same planform as the cathode surface is placed above the wall boundary layer to serve as a sustainer electrode. Fig. 3a shows the density disturbances due to the present of the plate in the supersonic flow without a discharge. A very thin boundary layer is observed as would be expected, because of the nearness of the leading edge. There is not much change in this boundary layer when the discharge is applied, if the plate serves as the anode. When an equal voltage with opposite polarity is applied, the boundary layer thickness triples (Fig. 3c). Increasing the power to the discharge results in an even thicker layer (Fig. 3d).

- 4 -

The oblique wave at the leading edge is clearly enhanced by the discharge in Figures 3c and 3d. The relative density jump across the wave changes from 5 to 15 percent when sufficient power is applied. This disturbance level can be predicted on the basis of the no flow results by the analogy between one-dimensional non-steady motion and two-dimensional supersonic flow (5).

By removing the cathode from the existing boundary layer and placing it in the core flow as shown in Fig. 3, the power loading per unit volume can be increased by a factor of two before arcing occurs. This is a significant improvement in the flowing gas case and suggests that additional gains are possible when boundary phenomena in discharges are fully understood.

REFERENCES

1. W.H. Christiansen, D.A. Russell, and A. Hertzberg, "Flow Lasers" in Annual Reviews of Fluid Mechanics 7,115 (1975).

2. B.B. O'Brien, Appl. Phys. Lett. 22,503 (1973).

3. E.R. Pugh, et al., Appl. Optics 13,11 (1974).

4. F.E. Culick, P.I. Shen and W.S. Griffin, IEEE J. Quan. Elec. QE-12, 10 (1976).

5. H.W. Liepmann and A. Roshko, Elements of Gasdynamics, p. 91 (1957), John Wiley & Sons, Inc., London.

11 mm

a.

14 mm

b.

c.

d

t = 30 μs

t = 38 μs

t = 72 μs

t = 130 μs
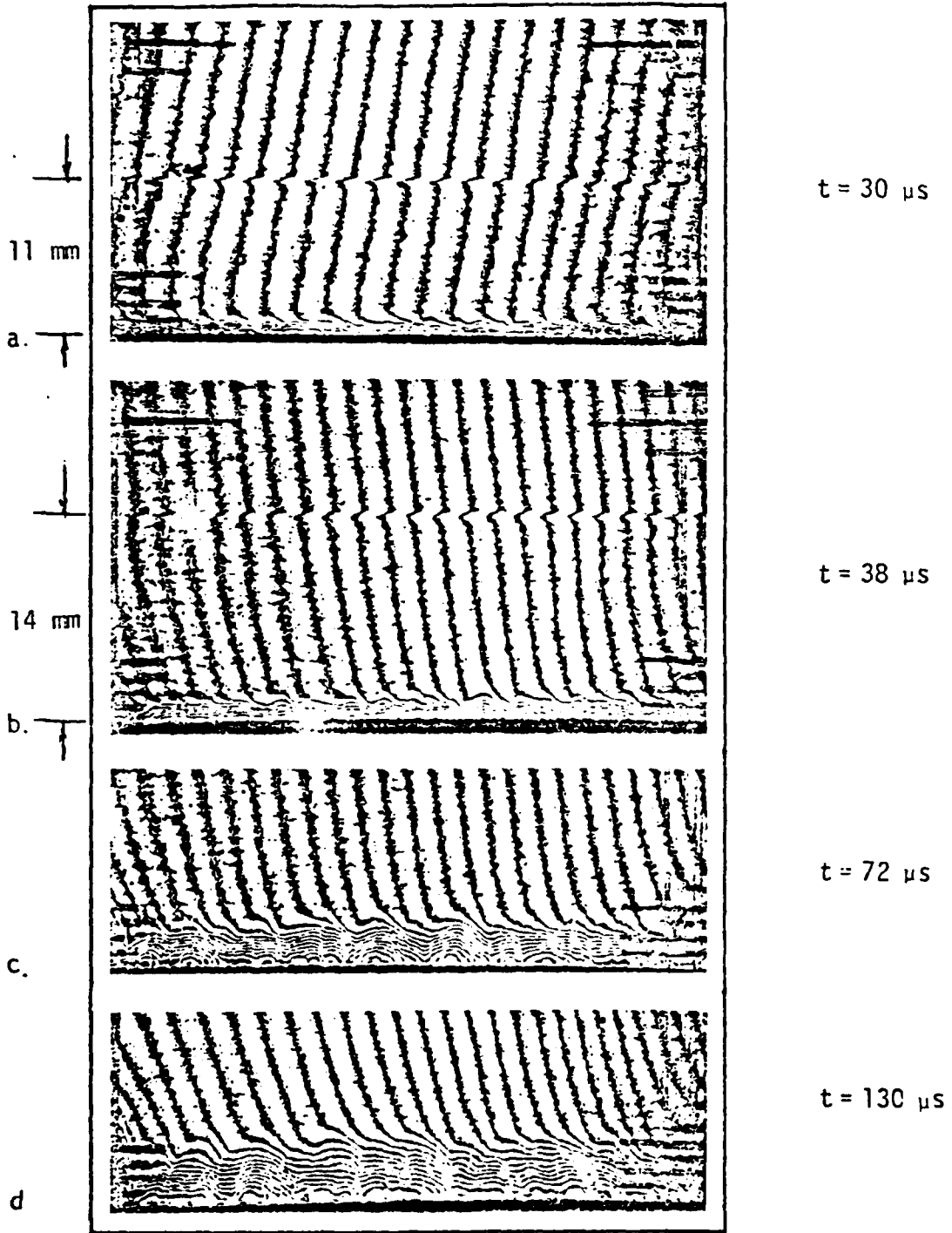
P = 300 torr N₂.

Fig. 1. Interferograms of the Density Disturbances at the Cathode in Static Discharge.
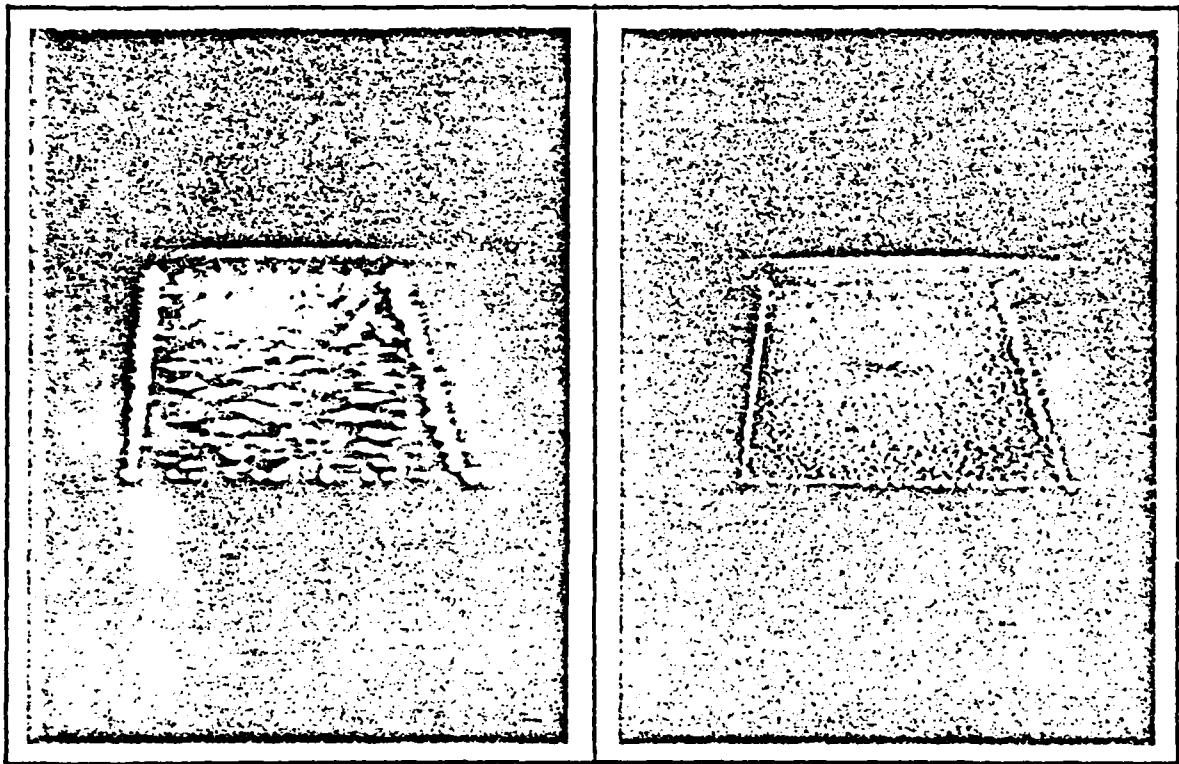
P = 100 torr   P = 300 torr

$t_{pulse} = 20 \ \mu s$

Fig. 2. Open Shutter Photographs of the Cathode Glow.

a. $\varepsilon = 0 \dfrac{\text{Joule}}{\text{lit.ama.}}$

b. $\varepsilon = 320 \dfrac{\text{Joule}}{\text{lit.ama.}}$

            ⟵ anode

c. $\varepsilon = 340 \dfrac{\text{Joule}}{\text{lit.ama.}}$

            ⟵ cathode

d. $\varepsilon = 650 \dfrac{\text{Joule}}{\text{lit.ama.}}$

            ⟵ cathode
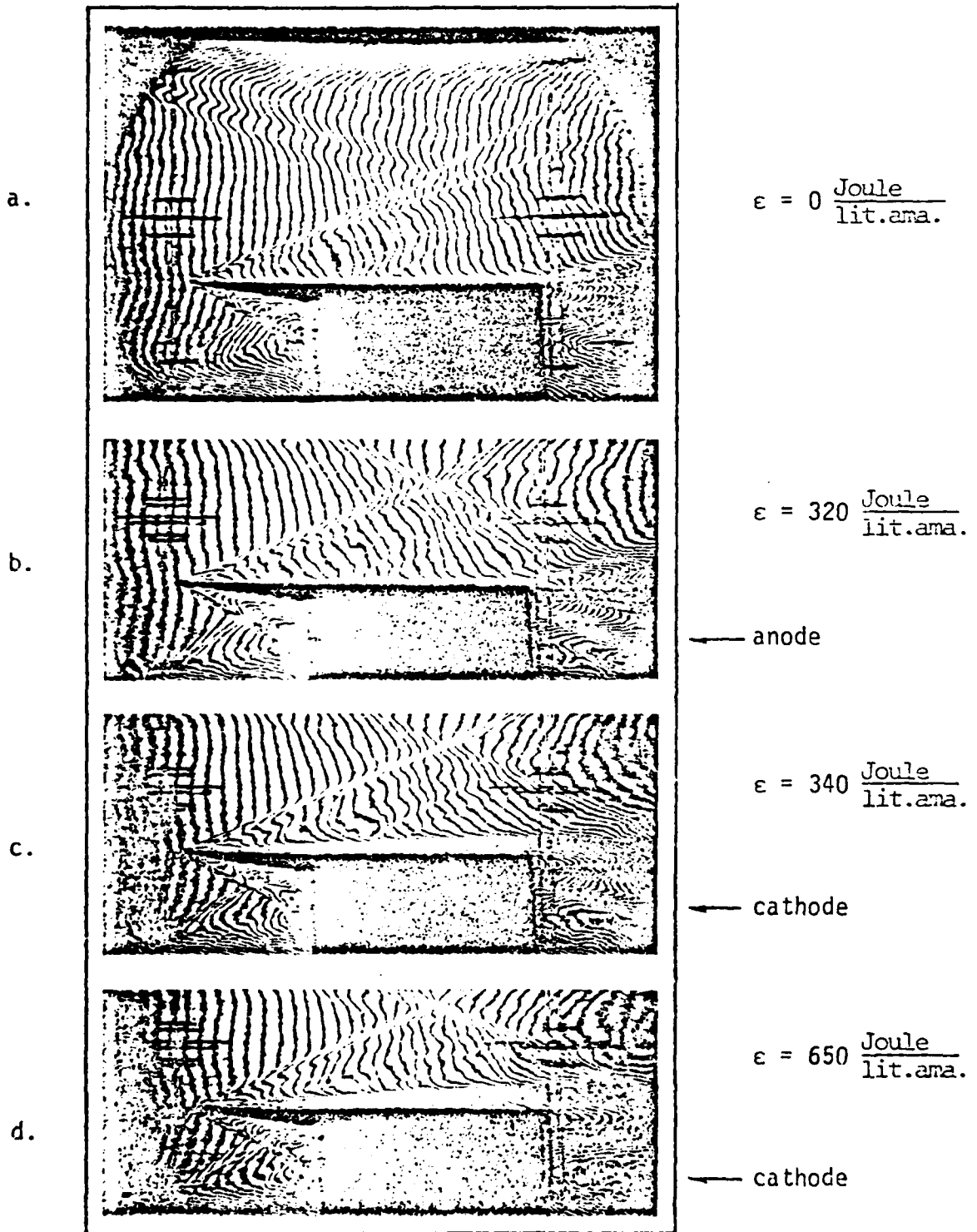
Fig. 3. Interferograms of the "Flying Electrode".

Appendix D

GASDYNAMIC LIGHT GUIDE

Introduction

The continuously varying refractive index field produced by a properly structured gas flow field can be used to manipulate light in a number of ways. For example, it is possible to create gas lenses, prisms, mirrors and light guides. The motivation for investigating such gas optics is twofold. First, very low losses, both reflection and absorption, are to be expected. Second, continuous operation at very high power levels (10^9 w/cm^2 or greater) should be possible.

The first work on gas lenses was at the Bell Telephone Laboratories[1,2,3]. The index differences in these lenses were created in very low speed flows at essentially atmospheric pressure either by modest temperature differences or by the use of two different gases. Very low speed flows were necessary to assure laminar flow during the diffusion of heat of gas specie. The refractive index gradients and the focussing power of these types of gas lenses, at least when operated at atmospheric pressure, are quite limited. Much higher index gradients can be created by gasdynamic means, as first suggested by Christiansen[4]. In particular, a properly designed radial flow supersonic nozzle (Fig. 1) can create, near the throat, a region which can act like a light guide closed in itself. Such a gas light guide can have a radius of curvature of 10 cm or less. This type of device has been named a Venus Machine, referring to conditions believed to exist on the planet Venus[5]. A complete (360°) Venus Machine could be used for the storage of light, or by using a gain medium as a working gas, as a mirrorless laser cavity. A partial Venus Machine, that is, a sector of angle, say, 90°, could be used to guide and deflect very high power laser beams.

The work to date at the University of Washington has included extensive calculations of Venus Machine characteristics, and investigation of the performance of a number of partial Venus Machines.

Theory

Theoretical analysis of a number of Venus Machine configurations are presented in detail in Refs. 6, 9, 10 and 11. This fairly general material will therefore be reviewed only briefly herein. More attention will be given at a later point to specific theoretical-experimental models used to interpret the data presented herein.

Diffraction is estimated to have only minor effects on light propagation in the Venus Machines discussed herein. Hence, the analyses are done using geometrical optics; the wavelength is assumed to be vanishingly small. If the index of a medium is known as a function of position, $n = n(\vec{r})$, the geometry of the wavefronts is determined by the eikonal equation[7], where

$$\nabla\psi \cdot \nabla\psi = n^2, \tag{1}$$

where the wavefronts are defined by the surfaces ψ = constant. For gases, the index, n, is related to the local density, ρ, by the equation[8]

$$n = 1 + \beta\rho/\rho_s, \tag{2}$$

where ρ_s is a reference density, usually taken at standard conditions. β is the Gladstone-Dale constant, which has the value 2.97×10^{-4} for nitrogen. If the medium has scalar electromagnetic properties, the direction of wave propagation is everywhere perpendicular to the wavefronts. Combining this fact with equation 1 yields the equation[7]

$$\frac{d}{ds}\left(n\frac{d\vec{r}}{ds}\right) = \nabla n \tag{3}$$

relating the coordinates of the ray path, $\vec{r}$, to the arc length, s, measured along the ray path. The cylindrical coordinate system shown in Fig. 1 will be used in the analysis which follows. It is assumed that the index, n, is a function of r and z only. From this point two approaches are taken in Refs. 6, 9, 10 and 11; these are discussed in A and B below.

A. nr Contour Plots

It is shown in Ref. 6 that an index field which has a local maximum of nr in a θ = constant plane creates, in the neighborhood of the maximum, a region capable of trapping and guiding light. Such a region is sketched in Fig. 2. The extent of this light well is defined by the largest closed nr contour not intercepted by the nozzle walls. This contour will be referred to as the limiting contour. Light trapped in the light well will, within the limits of the present analysis, remain trapped indefinitely. The light in the light well can deviate from motion in the pure θ direction up to a certain maximum angle and still remain trapped. The maximum deviation angle is a function of position inside the light well and is a maximum at the maximum of nr, where it can be shown to be given by

$$\psi \simeq \sqrt{2[(nr)_{max} - (nr)_{well\ boundary}]/(nr)_{max}} \tag{4}$$

The n and nr fields in a given nozzle can easily be calculated once the density field within the nozzle for the relevant operating conditions is known. Methods of calculating the two-dimensional inviscid compressible flow through a given nozzle profile are well known. For reasonable Venus Machine dimensions, Ref. 9 shows that two-dimensional solutions given a good approximation to the flow. Thus, given a Venus Machine nozzle profile, the operating gas, and the nozzle stagnation conditions, the n and nr fields can readily be calculated. nr fields for a variety of nozzle shapes and operating conditions are given in Refs. 9, 10 and 11.

B. Ray Tracing Calculations

For this type of analysis, the 3 scalar equations obtained from Eq.(3) and integrated numerically to yield ray paths around the Venus Machine for various initial conditions. Typically, an array of rays is considered to be injected in the neighborhood of the light well in the Venus Machine nozzle being considered. Results of this type of calculation are given in Refs. 6, 9 and 10. An important result of this type of calculation is that some rays injected close to, but outside of, the limiting nr-contour can remain "trapped" and guided by the Venus Machine for appreciable angles (e.g., 30°) but will eventually escape from the light well neighborhood. These rays are said to be partially trapped. The experimental work of Refs. 6 and 10 confirms the existence of appreciable partial trapping in 30° partial Venus Machines. Partial trapping will be discussed further in the detailed development of the model used to analyze the data presented herein.

C. Scattering

Light in the Venus Machine can be scattered by random density non-uniformities in the flow field. Four sources of density non-uniformities can readily be identified.

(a) Rayleigh scattering - scattering off acoustic modes in the flow, each one of which will have energy 1/2 kT, regardless of the flow quality.

(b) Scattering in the turbulent wall boundary layer.

(c) Scattering in the free stream flow due to boundary layer acoustic noise.

(d) Scattering in the free stream flow due to density non-uniformities convected to the light well from upstream separated flow regions.

(a), (b) and (c) are estimated to produce negligible effects for a 90° partial Venus Machine. (d) can be significant if the flow upstream

from the light well is of sufficiently poor quality. This is difficult
to assess. It is noted that (a) can never be eliminated; that (b) and
(c) could be eliminated only with laminar or relammarized boundary layer
flow; and that (d) could be eliminated by careful design of the flow channel
upstream from the light well.

Experimental Technique

The experimental work reported herein was performed in a 90° partial
Venus Machine. The nozzle shape is shown in Fig. 3; the throat height is
0.4 mm and the machine radius at the throat is 7.62 cm. The working gas
is nitrogen initially at room temperature. The nozzle stagnation pressure
drops continuously from 65-100 atm to about 30 atm during a typical
test.

A. Transmission Measurements

Fig. 4 shows a simplified sketch of the experimental setup. The beam
from a 1 mW HeNe laser is focussed down to a diameter of ~125μ and injected
into the Venus Machine on the nozzle symmetry plane. The position of the
input beam can be determined to ± .02 mm by using a 40x microscope. The
radial position of the center of the beam, taken as positive when measured
upstream from the nozzle exit, is defined as 1. Before entering the Venus
Machine, the laser beam is dropped at about 300 Hz and a portion is split
off and directed to the reference detector. Just before a test, the main
beam is deflected to the output detector by a calibrated prism; during a
test, the light is guided along the nozzle circumference to this same
detector. Comparison of the outputs of the two detectors on an oscilloscope
photograph, including data for some time before the test as well as that
during the test proper, allows calculation of the transmission at any time
during the test. The polarizers are used to zero out the difference channel
of the oscilloscope just before the test.

A Kistler pressure gauge in the Venus Machine gas reservoir is connected to a second oscilloscope. Timing marks applied to the cathodes of both oscilloscopes allow synchronization of the transmission and pressure data. The relevant stagnation quantity of the Venus Machine is the density, which can be calculated at any time during the test from the known blowdown characteristics of the reservoir-Venus Machine system. The quantity $R = \rho_0/\rho_s$, where ρ_0 is the stagnation density and ρ_s is the density at standard conditions will be used herein. The value of R at the beginning of a test is defined as R_0.

B. Photographic Data

The experimental apparatus is modified as shown in Fig. 5. For measurements of the output beam shape, the output plane of the Venus Machine is imaged on the ground glass and motion pictures are taken. The timing pulses sent to the pressure gauge oscilloscope are also used to drive the camera timing lamp, allowing synchronization of the photographic and pressure data. Care was taken to make the input beam position and the initial reservoir pressure be as close as possible for corresponding photographic and transmission tests. The distribution of the output beam in solid angle was determined using the same procedure with the imaging lens removed.

Some early (1974) photographic data is also discussed herein. The photographic technique for this data was very similar to that described above; the differences are as follows. A still camera was used and only one photograph was taken per test. The tests were very short, and $R = R_0$ for the photograph. Finally, the input laser beam was defocussed so the light well at the machine input was completely flooded with light.

The distribution of light in the light well measured photographically will be described herein primarily in terms of its maximum radial extent. The radial positions of the upstream and downstream limits of the lighted area, measureed from the nozzle exit with distances upstream taken as positive, are defined as j_e and k_e respectively. The angular distribution of light leaving the Venus Machine will be described primarily by ϕ_{er} and ϕ_{ez}, which are equal to half of the angular extent of the beam in the r and z directions, respectively. Under certain conditions, the output beam shows a long tail extending in the downstream r direction. The angular extent of this tail, measured from the estimated center of the light beam, is defined as ϕ_{eT}.

Initial Analysis of Data-Development of Model

Representative photographic data is shown in Fig. 6. Figs. 7, 8 and 9 present theoretical and experimental data on the radial distribution of light in the light well, the angular extent of the beam leaving the Venus Machine and transmission (T). The data of Fig. 7 was taken with the input of the Venus Machine flooded with light; that of Figs. 8 and 9 with the input beam focussed down to ~125μ diameter and injected at the indicated l values. The data of Fig. 7 was taken from the 1974 photographs; each test yielded only a single photograph and for all tests, $R \simeq R_0$. Each graph of Figs. 8 and 9 represents the data from one test, with R dropping continuously from 95 to about 30; in general, R is substantially less than R_0. Data discussed herein at a later point show that the experimental results are only slightly dependent on R_0; for this reason, the operating conditions of Figs. 7, 8 and 9 are considered identical. The experimental quantities j_e, k_e, ϕ_{er}, ϕ_{ez} and ϕ_{eT} were defined earlier. The circles in Fig. 7 are estimates of the location of the upstream limit of the light well obtained from early transmission

data runs by noting the R value at which the transmission dropped to 0.5. The hatched areas, j_s, j_n, k_s, k_n, ϕ_s, and ϕ_n are theoretically predicted limiting values which calculation is now discussed.

A simple one-dimensional model is used for the flow upstream of the nozzle exit. Due to the small size of the nozzle, rounding of the (ideally) sharp nozzle exit corners occurred during manufacture. Different degrees of rounding were noted at different locations in the nozzle. The one-dimensional flow calculations were made for cases which span the range of observed nozzle shapes. One case is ideal, with sharp corners and straight walls. In the second case, the throat is located .05 mm upstream of the exit, and the walls are curved near the throat. It was apparent early in the experimental program that the thermal boundary layers along the nozzle walls are important in the creation of light wells. The index at the wall was calculated with two different assumptions for the wall temperature; the first, the wall at the instantaneous adiabatic wall temperature and the second, the wall remaining at the initial temperature (530°R). The true wall temperature will lie somewhere between these two values. Downstream from the nozzle exit, the jet was, at first, taken to follow the inviscid free jet expansion from a sharp corner nozzle. A typical curve of nr versus r along the nozzle centerline obtained by these means is shown as the solid line in Fig. 10. (The curves of nr along the wall (nr_w), based on the adiabatic and constant wall temperature assumptions, are shown dashed.) Unfortunately, the optical data indicate a different behavior of the nr-r curve downstream from the nozzle exit; specifically, that the expansion occurs more slowly than the inviscid free jet calculation would indicate. The argument to this effect requires, as a prologue, the discussion of three separate points.

The first deals with random angular scattering in the Venus Machine. Under a number of different operating conditions, the output beam solid angle

distribution photographs showed well defined filamentary structures with angular widths as small as 0.5 degrees, roughly the subtended angle of the input laser beam. These filamentary structures were observed to change gradually over a number of motion picture frames and to be, to a considerable extent, reproducible between separate test runs. It is believed that these filaments represent a kind of extreme distortion of the laser beam as it traverses the Venus Machine. The existence of these filaments is a strong indication that the random scattering in the Venus Machine is less than, roughly, the half-width of the filament; that is, about 0.3 degrees. It is difficult to see how the existence of these filaments can be made consistent with a significantly greater random scattering.

The second point is that it is assumed that the nr-r curves along the nozzle centerline for different R values can be related by $n-1 \propto R$. There would appear to be no reason why the Reynolds number differences (factor of 2), and the differences in the temperature drop across the wall boundary layers should affect the expansion of the flow significantly. The final pressure to which the expansion goes is, of course, a smaller fraction of the nozzle stagnation pressure at higher R values; however, this should only affect the expansion far downstream of the light wells.

The third point involves a brief discussion of some aspects of partial trapping. Fig. 11 shows two representative nr contours in a typical Venus Machine light well. nr_1 is the limiting contour and nr_2 is a second contour further outside. The boundary layer thickness has been exaggerated for clarity. The motion of a representative partially trapped light ray in the r and z directions as it travels around the Venus Machine is shown. The ray is trapped by a number of reflections for a considerable time before it finds the saddle and escapes at point g. Estimates can readily be made of the number of reflections required before a random ray injected a

certain nr height above the limiting contour escapes. The number of reflections which occur as the light traverses the arc of the 90° Venus Machine is known approximately, leading to a simple estimate of the escape probability of a ray as a function of its nr height above the limiting contour at the point of injection. For the 90° Venus Machine, it can be shown that at the machine output, a significant amount of light can have remained partially trapped only a very short distance upstream of the upstream limiting contour.

It is well to mention at this point the behavior of a partially trapped light ray after it escapes through the saddle. Typically, such a ray can be shown to remain relatively close to the saddle for 20 to 30 degrees of Venus Machine arc, and then to move away in the direction of increasing r much more rapidly. The details of this motion depend, of course, on the well shape (the value of R) and on the point of injection of the ray. Under certain conditions, partially trapped rays which have escaped over the saddle, but are still close to the saddle, will be observed in the photographs and measured in the transmission data. This point will be returned to later in the paper.

The discussion of the expansion of the jet downstream of the nozzle exit is now continued, with reference to Figs. 7 and 10. The upstream limit of the lighted area at the Venus Machine exit, for the case with the machine input flooded with light (i.e., in Fig. 7) is taken, along with the transmission data points (circles), to determine the upstream limit of the light well. The specific curve taken is j_s in Fig. 7, reflecting both the transmission and photographic data. Taking the photographic data to determine the upstream limit of the light well requires the use of the first and third points discussed earlier. At the Venus Machine output, at the upstream edge of the lighted area, light could be observed upstream of the true light well limits for two reasons. First, the light could be partially trapped at the machine

input and transmitted to the area in question. The third point discussed
earlier indicates that this light should extend only a very small distance
upstream of the true light well limit. Second, light which is truly
trapped at the input of the Venus Machine could be scattered into the
area in question. From the earlier discussion of random scattering in
the Venus Machine, it can easily be shown that such light could extend,
at most, only a very small distance upstream of the light well limit.
Following these arguments, j_s in Fig. 7 is taken to determine approximately
the upstream limit of the light well. Turning to Fig. 10, for the nr curve
in question the j_s value determines point A. For most cases calculated,
the nr_{wa} and nr_{wc} curves in Fig. 10 lie below nr(A) and, hence, the
limiting point of the light well must be at the saddle, not at the wall,
and there must be a minimum of the nr curve downstream from the nozzle
exit at a point such as B, with nr(B) = nr(A). The location of B in
the r direction is not determined at this point. This type of calculation
can be made from the photographic data for values of R ranging from 50 to 95.
In all cases, the minimum of the nr curve (point B) indicated by the photo-
graphic data is very much above that calculated on the basis of an inviscid
free jet expansion (point H). This is the indication from the optical data
that the jet expansion downstream from the nozzle exit takes place significantly
more slowly than that based on the inviscid model. Up to this point, the
second of the three points presented earlier, the similarity of the nr
versus r profiles along the nozzle centerline, has not been used. It is
brought into play as follows. A number of different tangents to point B
are found, one for each different R value; these tangents can be collapsed
onto a single nr versus r curve using the similarity transformation. When
this is done, the tangents define a fairly self-consistent estimate of the

nr versus r curve downstream from the nozzle exit, up to a distance of about .3 mm from the exit. The location of the specific points B for each R value can now readily be determined from the "universal" transformed nr versus r curve.

The reasons for the relatively slow expansion downstream from the nozzle exit are not well understood at present. Boundary layer effects may be involved. It is also possible that, due to the Venus Machine construction, the effective back pressure at the nozzle exit is significantly above atmospheric. However, it is difficult to believe that this back pressure is sufficiently high to reduce the rate of expansion of the jet to that indicated by the optical data. The manufacturing errors, which are different at different places around the nozzle, further complicate the picture. Further investigation of the relatively slow expansion (compared to that calculated for a sharp corner nozzle with inviscid flow) indicated by the optical data was judged not to be profitable at present for the following reasons. First, the manufacturing errors would make any detailed analysis very difficult. Second, the relatively slow expansion indicated by the optical data leads to a consistent data analysis. Indeed, it is difficult to see how the expansion could be significantly more rapid and still produce the observed data. Finally, the light wells discussed herein for the 90° Venus Machine are of poor optical quality, and are only kinds of prototypes for future higher quality light wells.

Taking the nr-r curve downstream from the nozzle exit (dashed line in Fig. 10) to be determined from the photographic and transmission data as discussed above, the theoretical estimates of the limiting values of j, k and ϕ shown in Figs. 7, 8 and 9 can be obtained as follows. Reference is made

to Fig. 10. With j_s known, point B is determined and k_s follows directly.
This establishes the limits of the well based on light loss over the
saddle. For light loss at the walls, the nr_{wa} curve is taken as represen-
tative. Light is most readily lost at the walls in the neighborhood of
point F. The limits of the light well based on point F are obtained by
locating points C and D so that $nr(C) = nr(D) - nr_{wa}(F)$. The light well
limits based on loss at the walls were calculated for the cases of constant
wall temperature (nr_{wa} curve). Both saddle loss and well loss calculations
were done for the two different nozzle shapes discussed earlier. The range
of values obtained by these types of calculations is indicated for various
values of R by the j_s and k_s (saddle loss) and j_w and k_w (wall loss) hatched
areas in Figs. 7, 8 and 9. Where the k_w area crosses the k_s area, the former
cease. to exist. This corresponds to line EG in Fig. 10 which passes
below the saddle point B and does not generate a downstream well limit.
Finally, for either a saddle loss or wall loss calculation, the maximum
deviation of a trapped ray from the θ direction can be calculated as follows.
The adiabatic wall loss case in Fig. 10 is taken as an example. The maxi-
mum depth of the light well is Δnr_{wa}. The maximum angular deviation of
a trapped ray from the θ direction in this case can be calculated from the
following form of equation 4:

$$\phi_{wa} = \sqrt{2 \Delta nr_{wa}/nr(J)} \tag{5}$$

Similar calculations can be made for the constant wall temperature loss
case and the saddle loss case. The calculations are made for both nozzle
shapes considered. The ranges of ϕ values calculated by the methods for

various values of R are shown by the hatched areas in Figs. 8b and 9b. ϕ_w and ϕ_s are the wall loss and saddle loss calculations respectively.

From the upstream and downstream limits of the light well obtained as discussed above, the shape of the limiting nr contour for the case in question can be estimated. Such an estimation is discussed now for the case of a saddle loss calculation with reference to Fig. 12. j_s and k_s have been calculated and the solid part of the limiting contour can be sketched in directly. The dashed part of the contour can be roughly estimated from the photographs or from the calculations of Ref. 6, which are for inviscid flow through a sharp cornered nozzle. Since the photographic data includes light which is not trapped and also light leaving the well (as will be shown later) and the calculations of Ref. 6 are not directly applicable to the real flow situation, the dotted lines are only rough estimates. They do give, however, a general idea of the shape of the light well. The circles will be referred to at a later point in the paper.

One particular point of consistency of the light well model will be mentioned here. It will be recalled that the R value at which the transmission drops to 50% was used to obtain estimates of the upstream limits of the light well (circles in Fig. 7) which were in fairly good agreement with the limits as determined from the photographic data. Following the same procedure with the transmission data of Fig. 9c yields the square data point shown in Fig. 7, which is in good agreement with the k_s downstream limit determined as discussed earlier. The interpretation of this agreement is not as simple as would be the cure at the upstream limit, since the downstream limit is not a straight line as is the upstream, and partial trapping and limited guiding of light actually downstream of the saddle will be involved to a significant degree. However, despite these complicating factors, the good agreement does tend to support the model based on the experimentally determined upstream well limits.

Further Analysis and Discussion Based on Model

From Fig. 7, it can be seen that the experimental data used to determine the upstream limit of the light well based on the saddle calculation has little respect for the j_w limit for R greater than 85. Under other conditions, however, limiting values based on wall loss calculations are respected by the experimental data. An example of the latter is shown in Fig. 8b for R > 80, where the ϕ_{ez} and ϕ_{er} data give a strong indication of a wall loss limited light well. (See also later discussion.) Whether or not the data respects the wall loss limiting values depends on the location and nature of the light injection. Localized injection downstream of the nozzle exit tends to produce data which respects the wall loss calculations, whereas localized injection upstream of the nozzle exit tends not to respect these limits. The reason for this is not completely understood, but is probably related to the strongly curved nr contours downstream of the nozzle exit (e.g., see Fig. 11). Where "violation" of the wall loss limiting value occurs, the mechanisms is almost certainly as follows. In most cases, light injected into the well will immediately start oscillating strongly in the r direction. Oscillations in the z direction will then be gradually built up by repeated reflections off the curved nr contours downstream from the nozzle exit (e.g., the beam path in Fig. 11). Depending on the efficiency of the generation of z oscillations, these oscillations could remain considerably weaker than the r oscillations. Experimental evidence of r and z oscillations of unequal strength is shown in Fig. 9b for R > 80, where ϕ_{er} = 2.5 to 3.2 degrees, while $\phi_{ez} \simeq 1.9$ degrees. (The angular spread of the output beam is a good measure of the strength of the oscillations in the corresponding direction.) Loss of light through the saddle requires strong r oscillations while loss of light at the wall requires strong z oscillations. If the r oscillations are of a strength greater than the wall loss calculation limits, but the

z oscillations are weaker than this limit, light can appear in the well significantly upstream of the wall loss upstream limit, as noted in Fig. 7 for R > 80. It should be noted here that reflection off the metal walls of the nozzle is sufficiently poor not to be an option to reflection off the boundary layer.

In the data of Fig. 8 for 45 < R < 57, and in the data of Fig. 9 for 52 < R < 70, the following characteristic behavior is noted. j_e is closely equal to j_s, and k_e is much greater than k_s. ϕ_{er} and ϕ_{ez} are in the range of the ϕ_s limiting values, while for some R values, a tail of light occurs with ϕ_{eT} much greater than ϕ_s or ϕ_w. The transmission drops very steeply in the ranges of R values discussed. In each case this characteristic behavior occurs at the R values where the j_s or k_s limits (which move inwards as R decreases) are moving past the location of the input laser beam. A consistent picture may be drawn from this data as follows. Under the conditions in question, some light is injected right up to the limiting nr value of the well (the saddle loss limit, since the wall loss limit is less restrictive) filling the well and producing oscillations, in the r direction at least, of strengths up to the limiting value. Thus, j_e is expected to be equal to j_s and ϕ_{er} is expected to be equal to the limiting value ϕ_s, as is observed. Since light is also injected above the limiting nr value, partial trapping will occur and light will be observed at the Venus Machine output which is outside the light well and is either partially trapped upstream of the saddle or is in the process of escaping from the well downstream of the saddle. (Contributions to the light observed outside the light well can also be made through scattering of truly trapped light through small angles.) This is observed experimentally through the observation of light downstream of the saddle ($k_e > k_s$) and travelling at angles to the θ direction substantially greater than ϕ_s (the tails with $\phi_{eT} > \phi_s$ and ϕ_w). The spatial extent and intensity of the light observed

outside the light well proper are roughly consistent with that expected
on the basis of estimates of the amount of partial trapping, the rate of
escape of partially trapped light and the motion of the light after it
escapes from the well. Finally, since the j_s or k_s limits are moving inwards
past the center of the injected beam, a steep drop in T is to be expected
and is observed.

For the case with the input of the Venus Machine flooded with light,
there will, of course, be injection of light above the well limit for all
values of R. The observation of light at the Venus Machine exit which
is outside the light well proper is indicated by $k_e > k_s$ for R < 85. Again,
the extent and amount of light observed outside the light well proper is
roughly consistent with that estimated analytically. A word of caution should
be given with respect to a possible comparison of the k_e curve of Fig. 7
with those of Figs. 8 and 9. When a focussed beam is injected near the
limiting nr contour, the quantity of light partially trapped can be much
larger relative to that truly trapped than for the case with the machine
input flooded with light. For this reason, problems of film exposure prevent
the k_e curve in Fig. 7 from being closely comparable to the curves of Figs. 8
and 9. This is very likely the reason why the k_e values of Fig. 7 are smaller
than those of Fig. 8 for R < 55 and of Fig. 9 for R < 70. This effect may
also be involved in the apparent lack of light outside the light well proper
shown in Fig. 7 for R > 85. In this case, however, loss at the wall may
provide some restraining effect on k_e, though, as discussed earlier,
insufficient to bring k_e into the k_w range.

A few general observations from Figs. 7, 8 and 9 are now noted.
For localized injection, the upstream limit of the lighted area, j_e, is
equal to, or inside of, the corresponding limit with the input of the Venus
Machine flooded with light. This is to be expected, since the flooded input
lighting conditions could be regarded as including the localized

injection conditions as components. For localized injection, the downstream limit of the lighted area, k_e, respects the k_s limits except for those R values discussed earlier, where substantial amounts of partial trapping occur. This again is an expected result, since, if significant partial trapping is not indicated by any of the remaining data, most of the light should be well contained in the well and therefore should not extend beyond the k_s limit. Finally, an examination of the ϕ data of Figs. 8 and 9 shows that, except for the ϕ_{eT} (tail) data, ϕ_s and ϕ_w give good sets of limiting values, with the experimental data tending towards the upper parts of the limiting bands for certain R values. For $l = -.15$ mm, $80 < R < 95$, ϕ_w is limiting, and for $l = -.15$ mm, $47 < R < 63$ and $l = .20$ mm, $57 < R < 70$, ϕ_s is limiting.

A number of aspects of the experimental data of Figs. 8 and 9 are organized in Table 1. This table also includes a description of the appearance of the solid angle beam distribution photographs taken at the output of the Venus Machine. The data of Table 1 can consistently be interpreted in terms of whether the beam is injected high up in the light well, near a limit, or lower in the well, further from the limits. For injection high in the well, near limiting values (j_s, k_w, k_s), cases 2, 3 and 5, the following picture can be drawn. Part of the light oscillates with strengths at or near the maximum permissible values (i.e., ϕ_{ez} and $\phi_{er} \simeq \phi_s$ or ϕ_w), and the well is essentially filled to the limiting nr contour, and possibly to slightly above this contour, if partial trapping occurs. The strong oscillations are very probably responsible for the following. First, relatively good communication between the r and z oscillations occurs in the well and hence $\phi_{er} \simeq \phi_{ez}$. Second, most of the light structure in the well is destroyed, leading to very disorganized solid angle beam distribution photographs (though filamentation was observed to occur for Case 2). Since the input beam is of finite extent, some of

the light is not trapped and the transmission is relatively low. For injection lower in the well (Cases 1 and 4) the following picture obtains. First, it should be noted that the data indicate that Case 4 is not as low in the well as Case 1. The injection for Case 4 can be considered to be inside the k_w limit only if the innermost part of the k_w band is ignored. Also, ϕ_{er} and ϕ_{ez} are not truly below the ϕ_s limiting band but are only located in the lower half of the band. With these caveats, the following picture is drawn for injection low in the well, well inside the j_s, k_s and k_w limits. The well is filled only to a level significantly below the limiting contour and the oscillations are of strengths considerably weaker than the maximum permissible. The latter point is well illustrated for Case 1, where ϕ_{er} and ϕ_{ez} are considerably less than ϕ_s and ϕ_w; for Case 4, as mentioned above, ϕ_{er} and ϕ_{ez} are not definitively below the ϕ_s band. The weaker oscillations are almost certainly responsible for the fact that the structure in the light well is not completely destroyed and appears as banding in the solid angle beam distribution photographs. For Case 1, the structuring is also apparent in the fact that ϕ_{ez} is significantly less than ϕ_{er}. Since the input beam is located well inside the well, most of the light is trapped and the transmissions are relatively high. For the high transmission conditions of Fig. 9 with $1 = .20$ mm, the input laser beam is located in the light well with respect to the well limits roughly as shown by the left hand circle in Fig. 12. Fig. 12 also shows, by the right hand circle, roughly how the laser beam is located in the well for the high transmission conditions of Fig. 8, with $1 = -.16$ mm. The better placing of the input laser beam in the former case almost certainly accounts for the higher transmission ($T_{max} > .99$) observed for $1 = .20$ mm compared to that observed for $1 = -.16$ mm ($T_{max} \approx .95$).

TABLE 1

Case	1	2	3	4	5
1, mm	.20 (Fig. 9)	.20	-.16 (Fig. 8)	-.16	-.16
R	75-95	55-75	80-95	60-80	45-60
relation of point of injection to limits	well inside j_s, j_w	nearer to or at j_s	at or near k_w	inside k_s, slightly inside (mean value of) k_w	at or near k_s
relation of ϕ_{ez} and ϕ_{er} to limits	well under ϕ_s, ϕ_w	high in ϕ_s band	high in ϕ_w band	under ϕ_w lower in ϕ_s band	high in ϕ_s band
is ϕ_{ez} less than ϕ_{er}?	yes	no	no	no	no
relative value of transmission	very high	lower	lower	high	lower
appearance of solid angle beam distribution photographs	strong structure, banded	disorganized (though with filaments)	disorganized	strong structure, banded	disorganized
classification of location of input beam in well	very low	high	high	moderately low	high

The maximum transmission value shown in Fig. 9c is .997. Four earlier runs with 1 = .18 to .24 mm taken with a somewhat inferior method of determining the position of the input laser beam indicated maximum transmission values of .981, .990, 1.000 and 1.003. The variability of the maximum values is very likely due to the extreme sensitivity of the Venus Machine to the exact location of the input laser beam. For any given transmission value, the following is the estimate of the experimental accuracy.

Error in determining the transmission of the reference prism	$\pm$ .002
Errors due to possible interference effects in the input and output windows	$\pm$ .0025
Error in reading data off oscilloscope pictures	$\pm$ .001-.002
Errors due to inaccuracies in the gains of the recording oscilloscope (not measurable)	$\sim$ 0
Total estimated error	$\pm$ .0055-.0065

Thus, the maximum measured transmission can be written as 1.003 $\pm$ .0065, or, more realistically, .998 $\pm$ .002. The investigators prefer to make the slightly more conservative statement that the maximum transmission is greater than .995.

All data discussed up to this point (except for the 1974 photographic data) were taken with $R_0 \simeq 95$. With $R_0 \simeq 68$, transmission data was also taken for 1 = -.16 mm, and 1 = .20 mm, and photographic data was taken for 1 = -.16 mm. A discussion and comparison of the $R_0 \simeq 95$ and $R_0 \simeq 68$ data follows. Since data with $R > 68$ is not available in the test runs with $R_0 \simeq 68$, the comparison is limited to values of R below 68. For a given value of R, greater temperature differences between the free stream and the well will exist at the higher values of R_0. The following effects of

the temperature differences on the light well might be expected to exist. First, the wall thermal boundary layer would tend to provide greater stabilization of the light well at the higher values of R_0. Second, of the four causes of scattering in the light well mentioned previously, scattering in the boundary layer and scattering in density non-uniformities in the free stream convected from separated flow regions would be larger at the higher values of R_0, due to the larger temperature differences. Experimentally, the photographic data were almost identical for $R_0 \simeq 68$ and $R_0 \simeq 95$. For both $l \simeq -.16$ mm and $l \simeq .20$ mm, the transmission data were very similar for $R_0 \simeq 68$ and $R_0 \simeq 95$; however, the rapid fall-off of transmission did occur at slightly lower values of R for $R_0 \simeq 68$. The difference was ΔR (fall-off) $\simeq 1$. The difference in ΔR (fall-off) may well be due to slightly increased scattering for the cases with $R_0 \simeq 95$. Such increased scattering at higher values of R_0 is unconfirmed by any other experimental data at present.

Concluding Remarks

It is not appropriate to attempt to summarize the foregoing detailed discussion of the experimental results here. However, several points judged to be of more general interest are given below.

(1) The operation of the existing 90° Venus Machine is fairly well understood, although there are still points on which further work needs to be done.

(2) The 90° Venus Machine can operate at transmissions greater than .995.

(3) There are strong indications that the random angular scattering in the 90° Venus Machine is less than 0.3 degrees.

(4) The relatively large size of the output beam of the existing 90° Venus Machine (typically about 4 degrees half angle) is due

(a) errors in the manufacture of the machine, for example, rounding of the sharp corners of the nozzle exit; and (b) the fundamentally very poor shape of the light wells (e.g., Fig. 12), which tend to severely distort the input laser beam. A more suitable well shape would approximate that of a graded index fiber.

(5) From the theoretical work of Refs. 6, 9, 10 and 11 and the experimental work discussed herein, it appears to be feasible to construct in the future, gasdynamic light guides of much higher optical quality, which light well shape will approach that of a graded index fiber.

REFERENCES

1. D.W. Berreman, Bell Syst. Tech. J. 43, 1469 (1964).

2. D.W. Berreman, Bell Syst. Tech. J. 43, 1476 (1964).

3. D. Marcuse and S.E. Miller, Bell Syst. Tech. J. 43, 1759 (1964).

4. W.H. Christiansen, Bull. Am. Phys. Soc. 11, 1594 (1968).

5. V.R. Eshleman, et al., Science 158, 1678 (1967).

6. W.H. Christiansen and A.P. Bruckner, Applied Optics 14, 1556 (1975).

7. M. Born and E. Wolf, "Principles of Optics" (Pergamon Press, New York, 1970), pp. 112, 122.

8. H.W. Liepmann and A. Roshko, "Elements of Gasdynamics" (Wiley, New York, 1957), p. 154.

9. W.E. Frederick, "A Fluid Mechanical System for the Storage or Deflection of a Laser Beam," M.A.A. Thesis, Department of Aeronautics & Astronautics, University of Washington, Seattle (1971).

10. C. Gantet. "Study of the Trapping of Light by the Venus Machine," M.S. Thesis, Department of Aeronautics & Astronautics, University of Washington, Seattle (1973).

11. M.J. Dunn, "Analysis and Design of Gasdynamic Lightguides," M.A.A. Thesis, Department of Aeronautics and Astronautics, University of Washington, Seattle (1974).
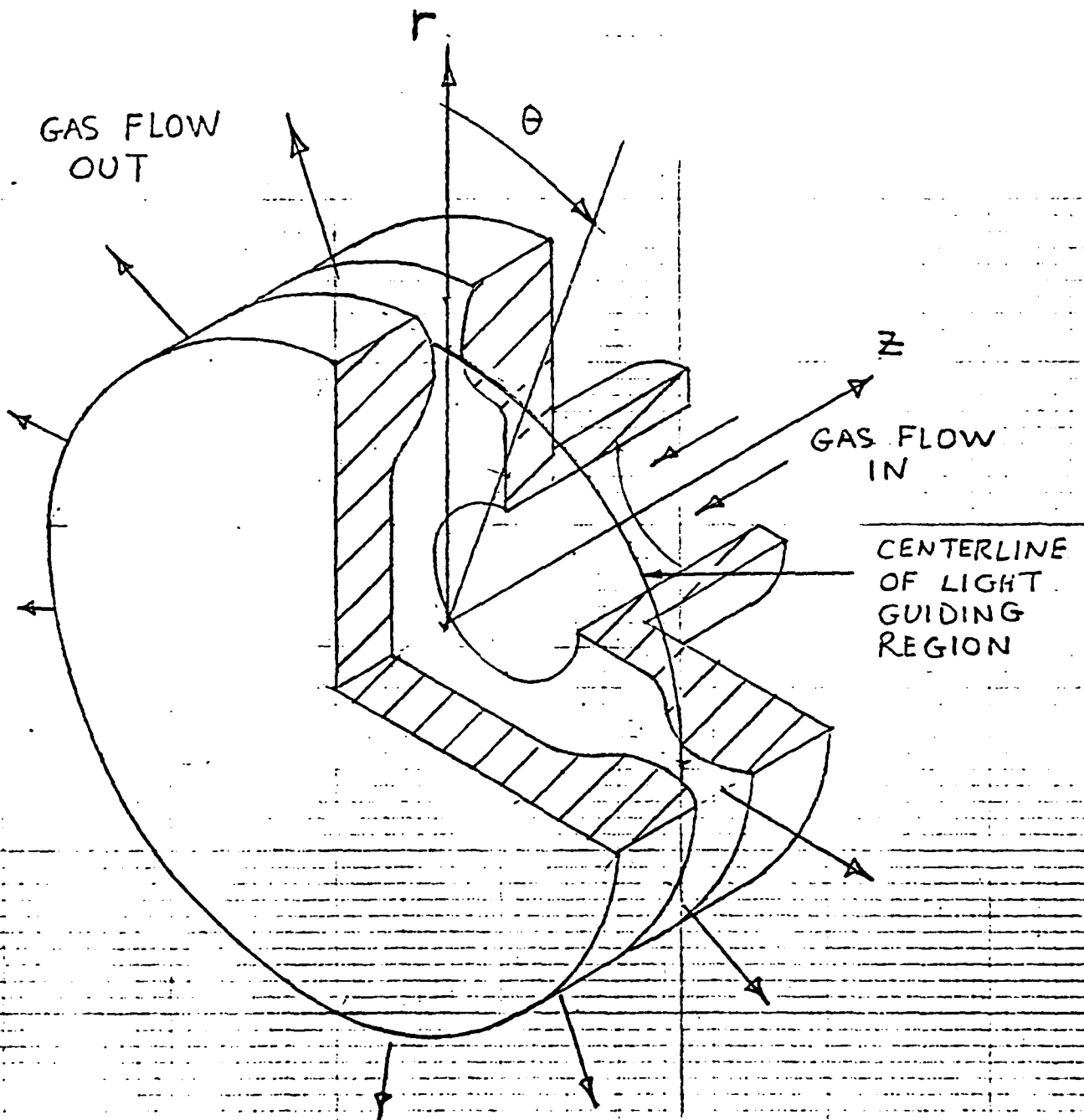
FIGURE 1

360° Venus Machine and cylindrical
coordinate system.
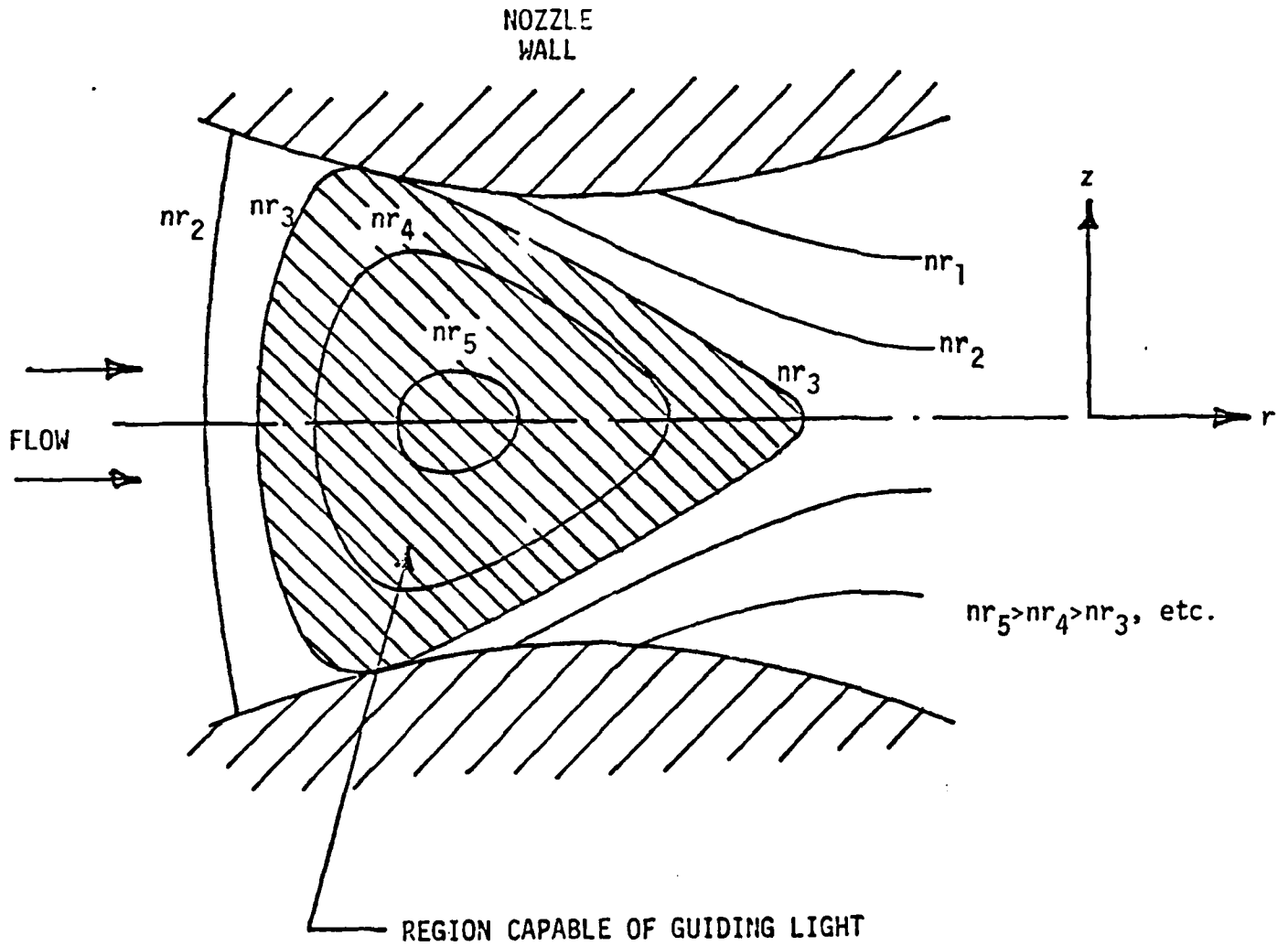
Figure 2. Typical region in a convergent-divergent nozzle capable of guiding light.
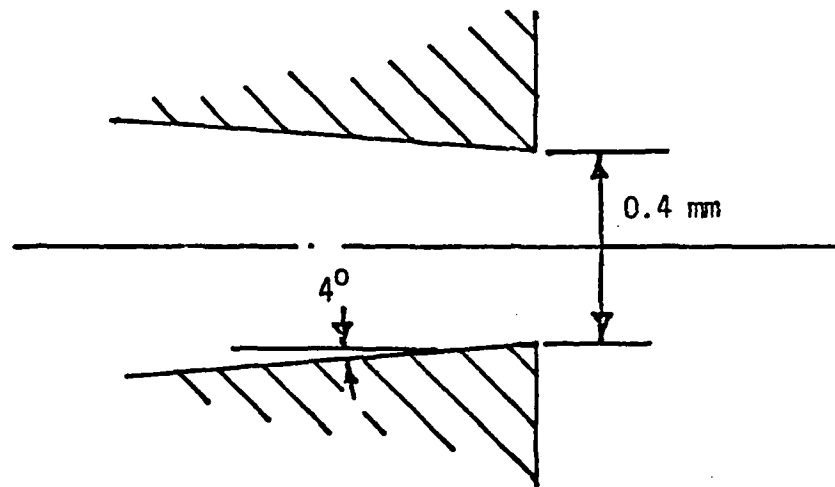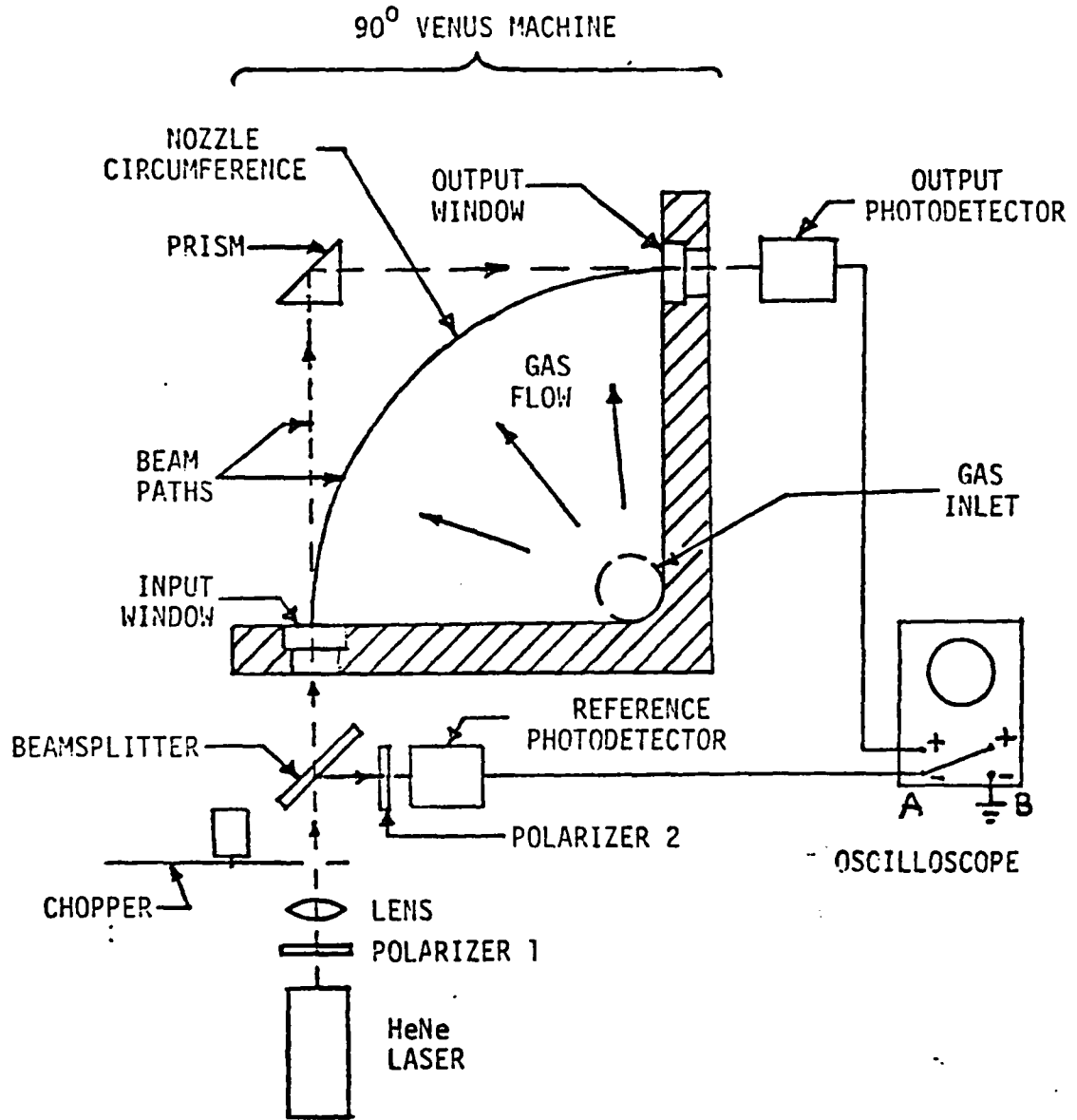
Figure 3. Shape of nozzle in 90° Venus Machine.

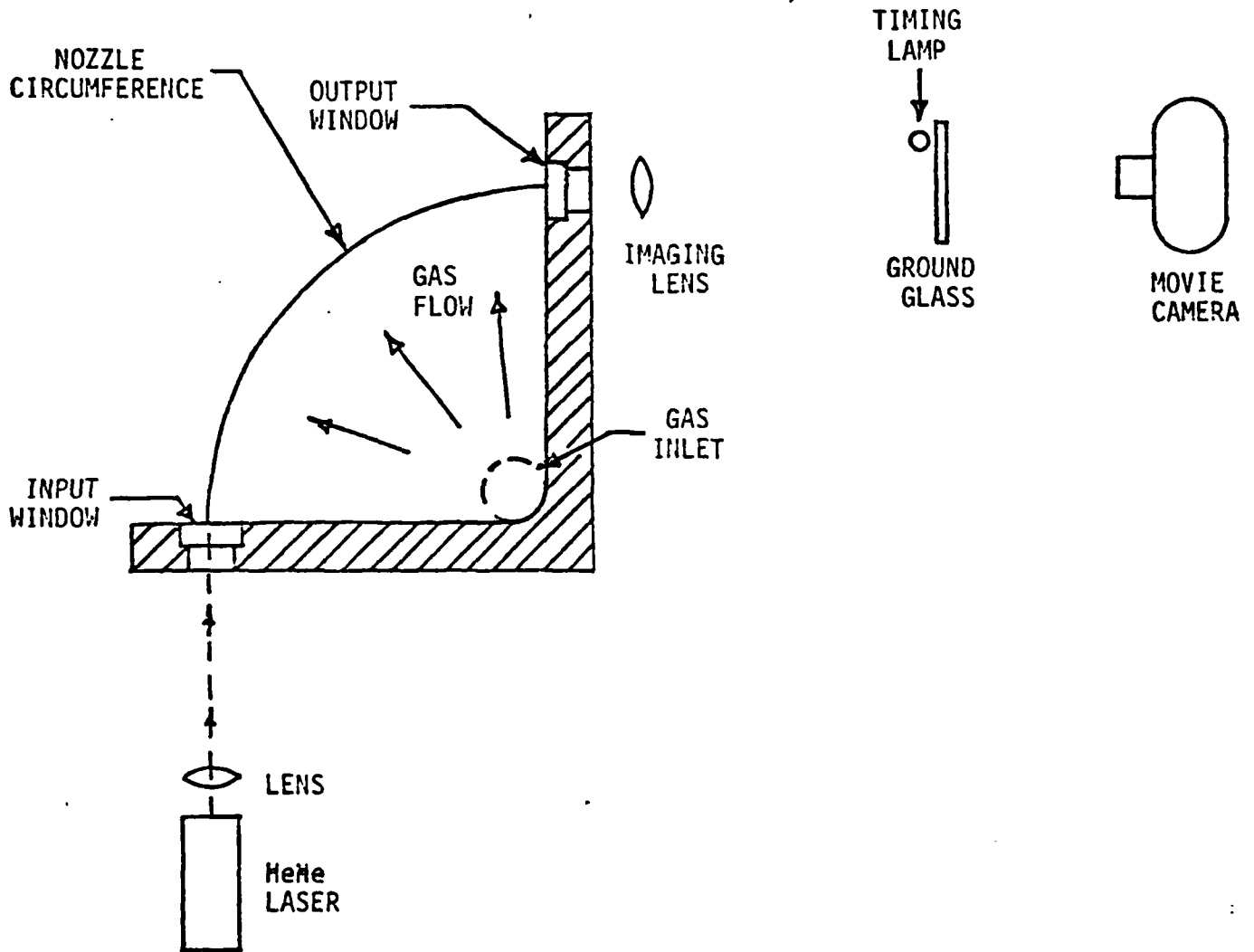Figure 4. Experimental setup for beam transmission measurements on the 90° Venus Machine.

Figure 5. Modification of the experimental setup
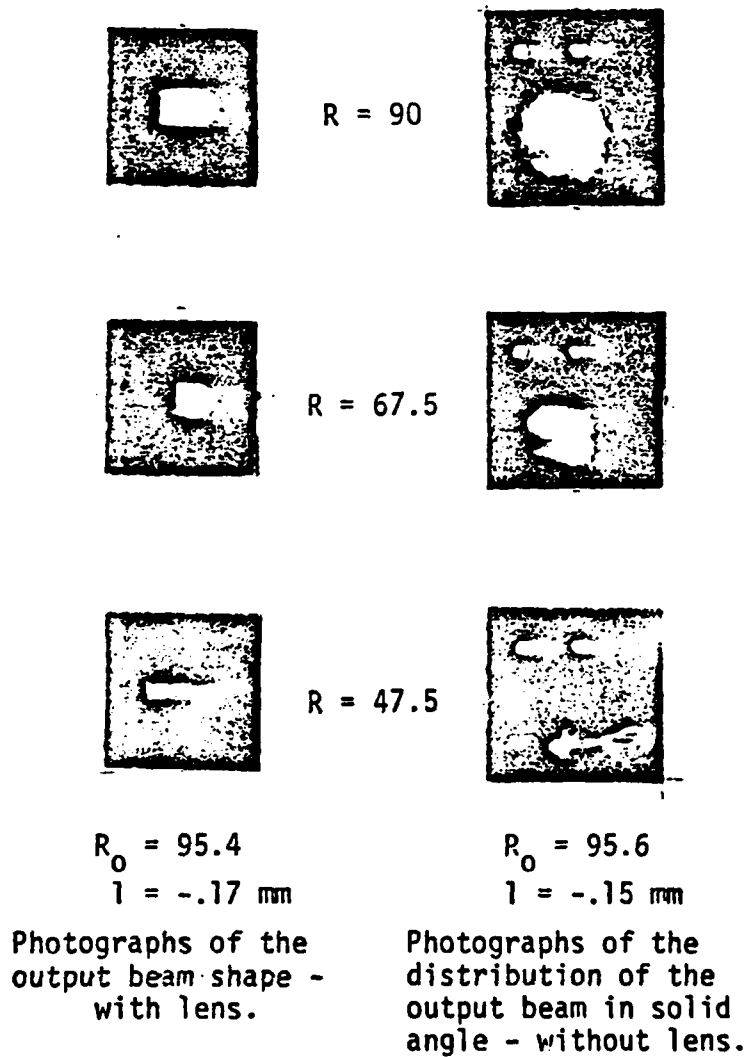for the taking of photographic data.

R = 90

R = 67.5

R = 47.5

R_o = 95.4
1 = -.17 mm

R_o = 95.6
1 = -.15 mm

Photographs of the
output beam shape -
with lens.

Photographs of the
distribution of the
output beam in solid
angle - without lens.

Figure 6. Representative photographic data.
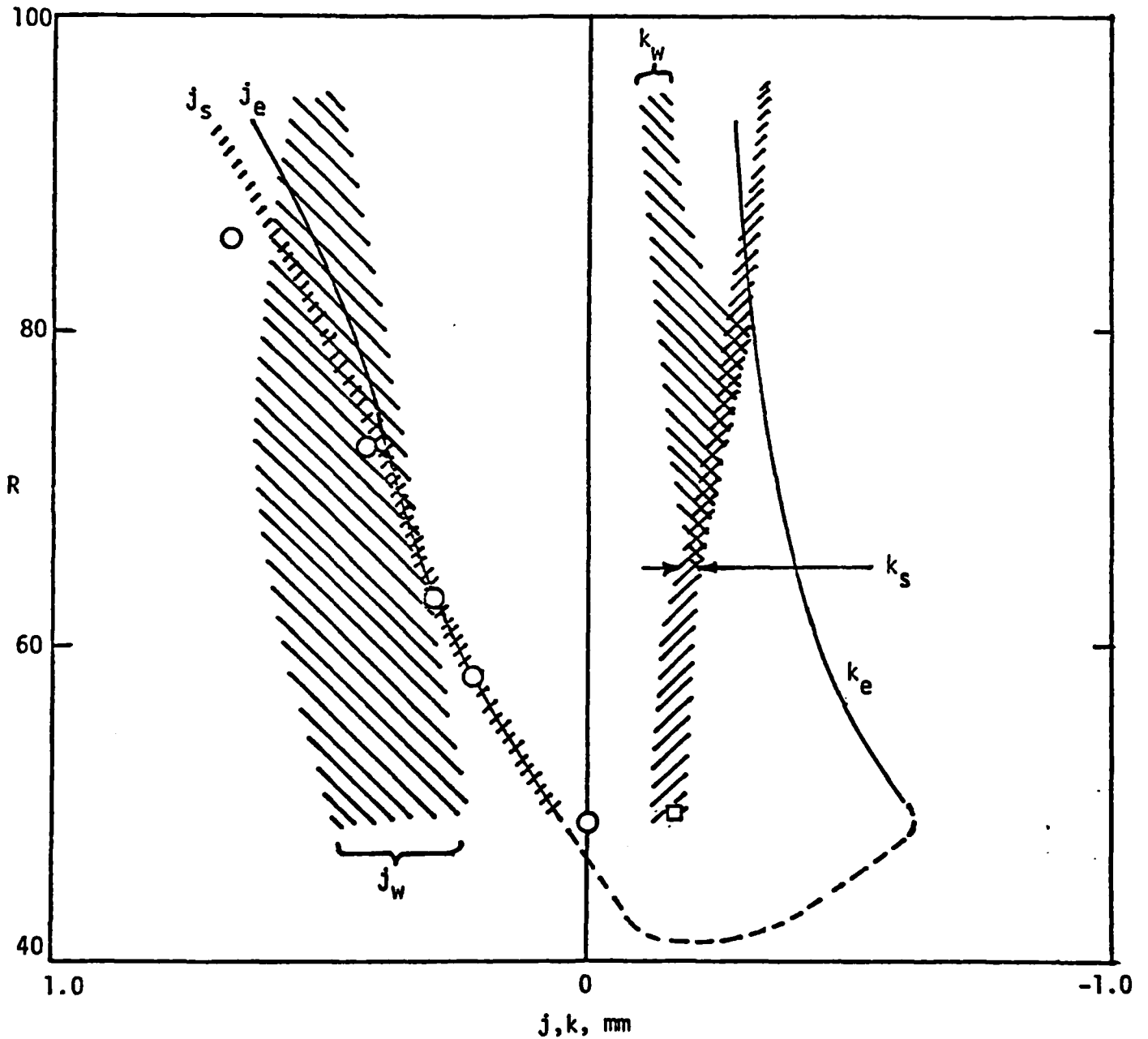
Figure 7. Comparison of theoretical and experimental
results for the radial extent of the lighted area at
the output of the Venus Machine. Venus Machine input
flooded with light.
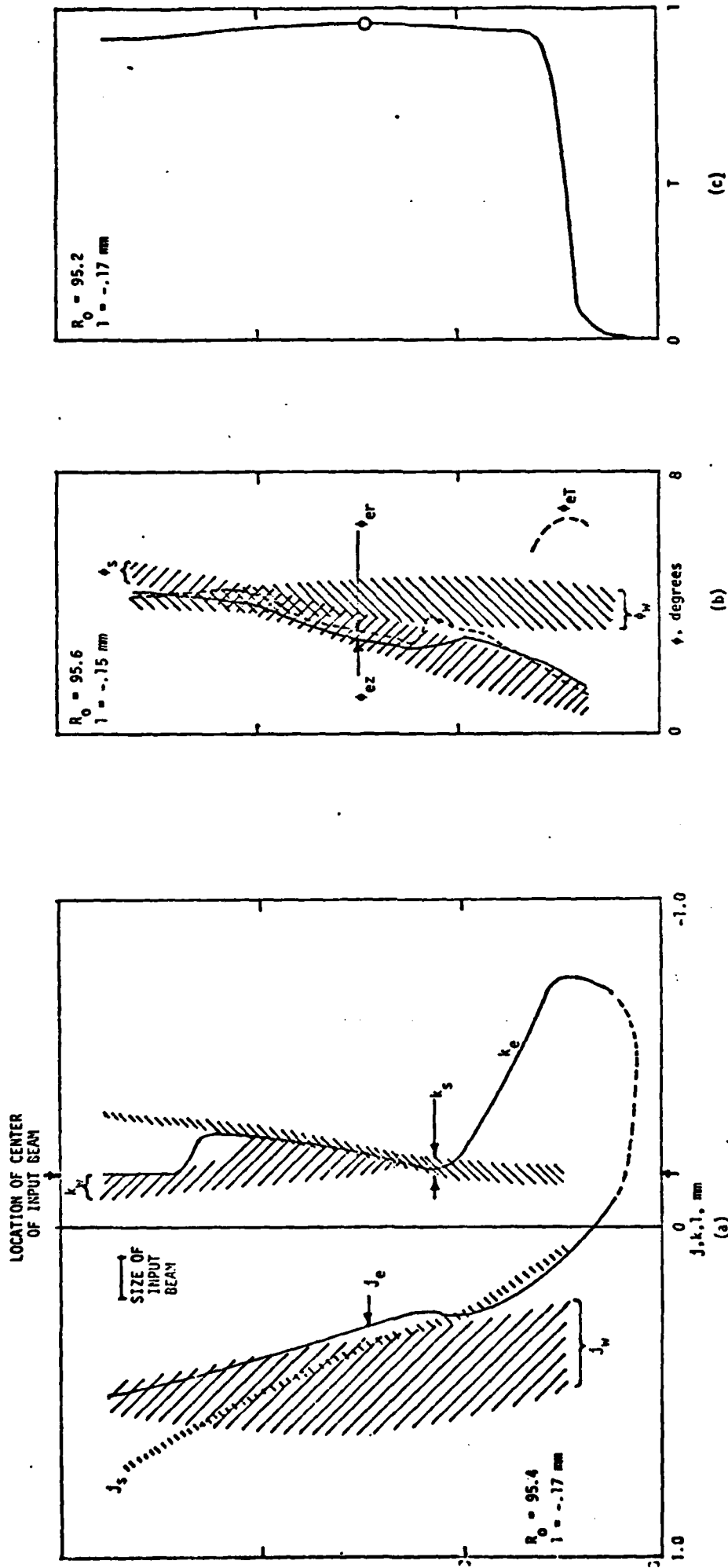
Figure 8. Comparison of the theoretical and experimental results for the radial extent of the lighted area at the output of the Venus Machine, and the distribution of the output beam in solid angle. Transmission data is also shown. Light input into the Venus Machine localized at l = -.16 mm.
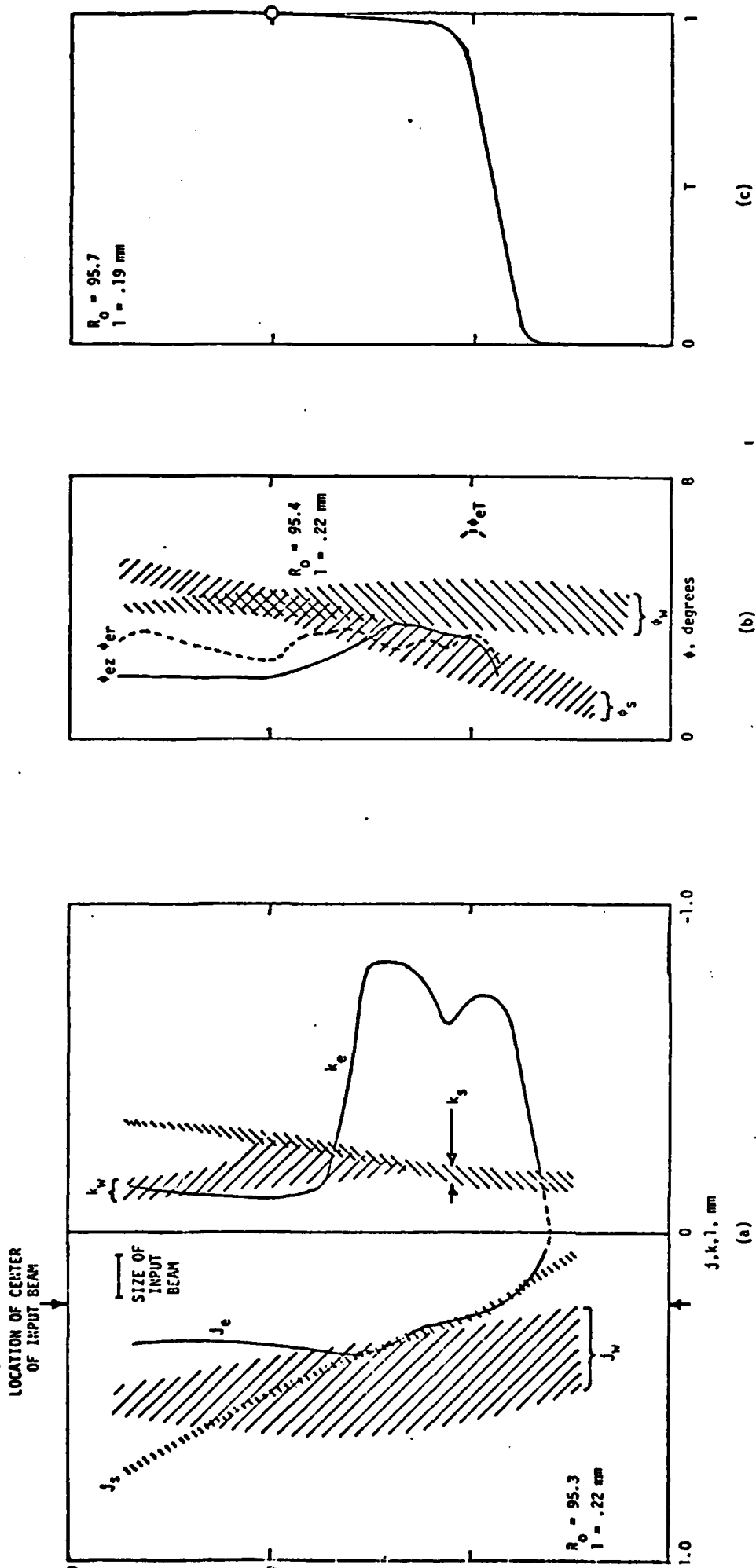
Figure 9. Comparison of theoretical and experimental results for the radial extent of the lighted area at the output of the Venus Machine, and the distribution of the output beam in solid angle. Transmission data is also shown. Light input into the Venus Machine localized at 1 = .20 mm.
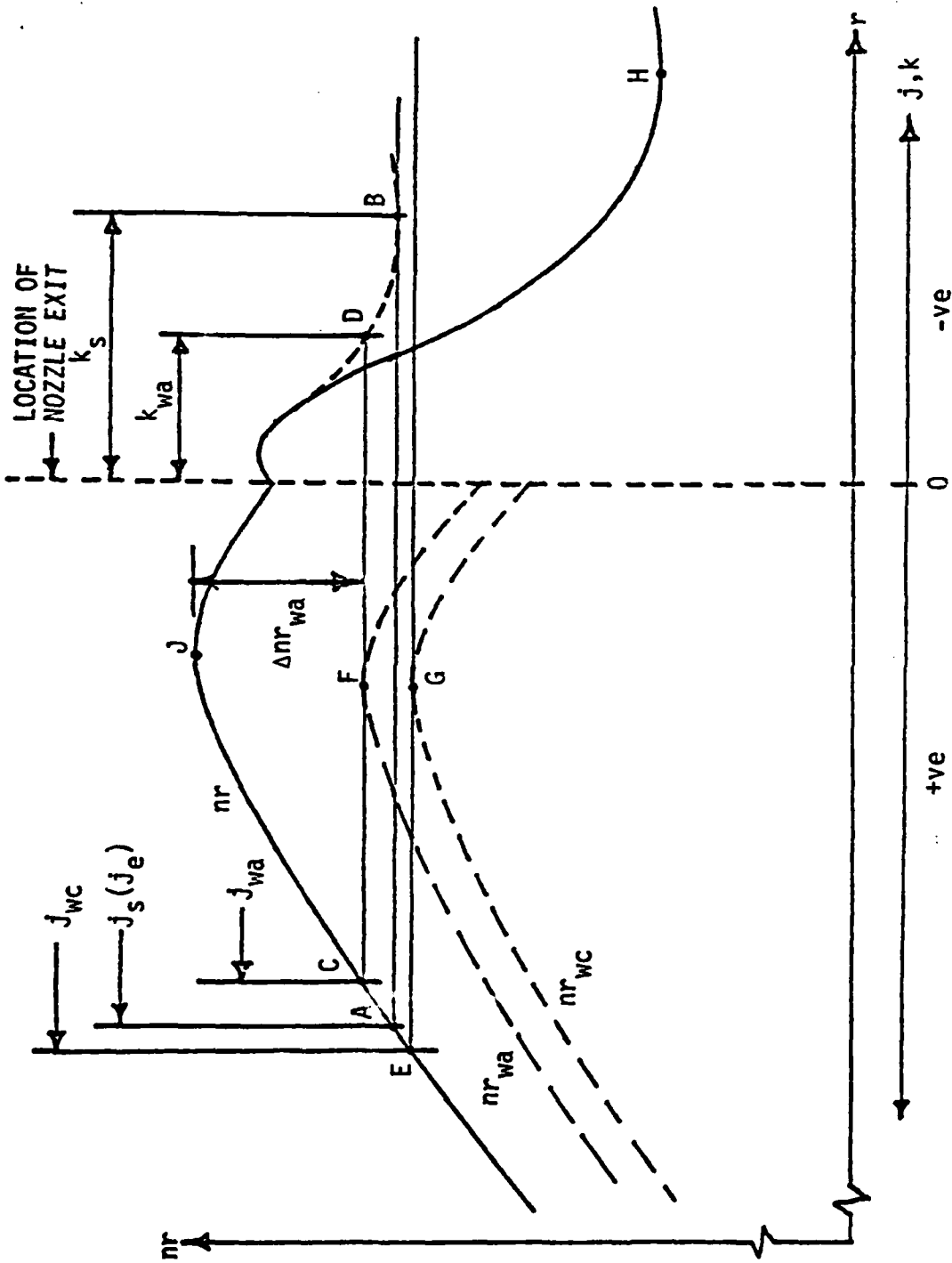
Figure 10. Theoretical and theoretical-experimental curves of nr versus radius in the Venus Machine. Curves are shown both along the nozzle centerline and along the nozzle wall. The curves are used in the development of the model used in the interpretation of the experimental data.
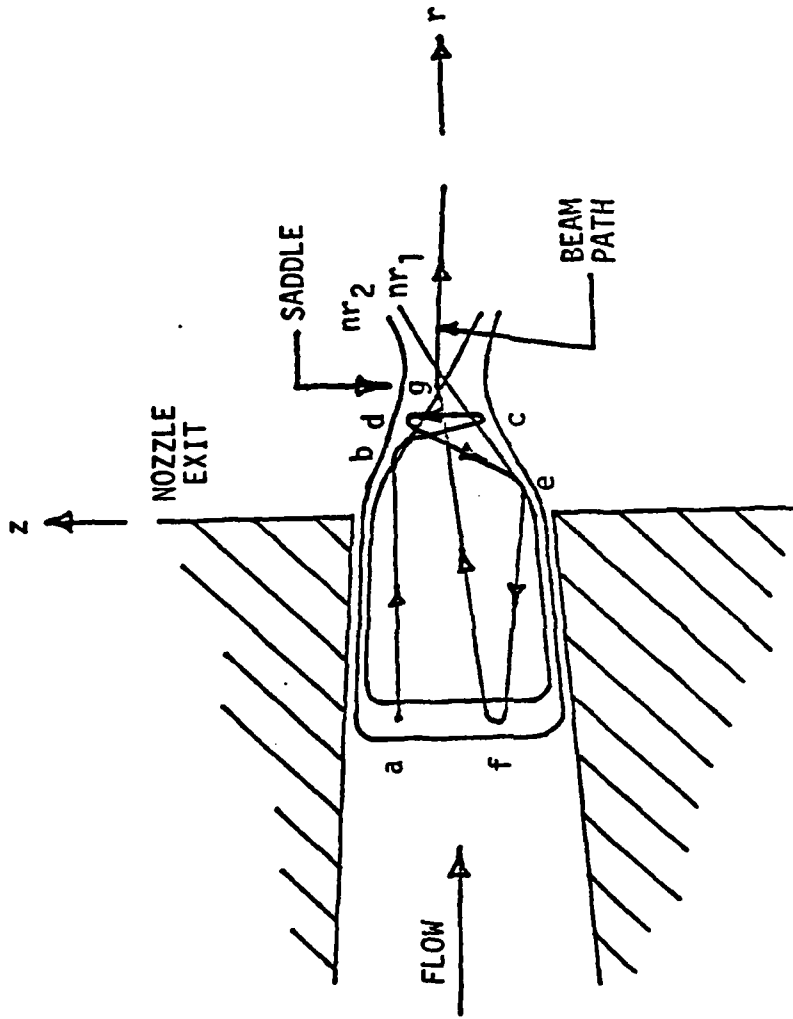
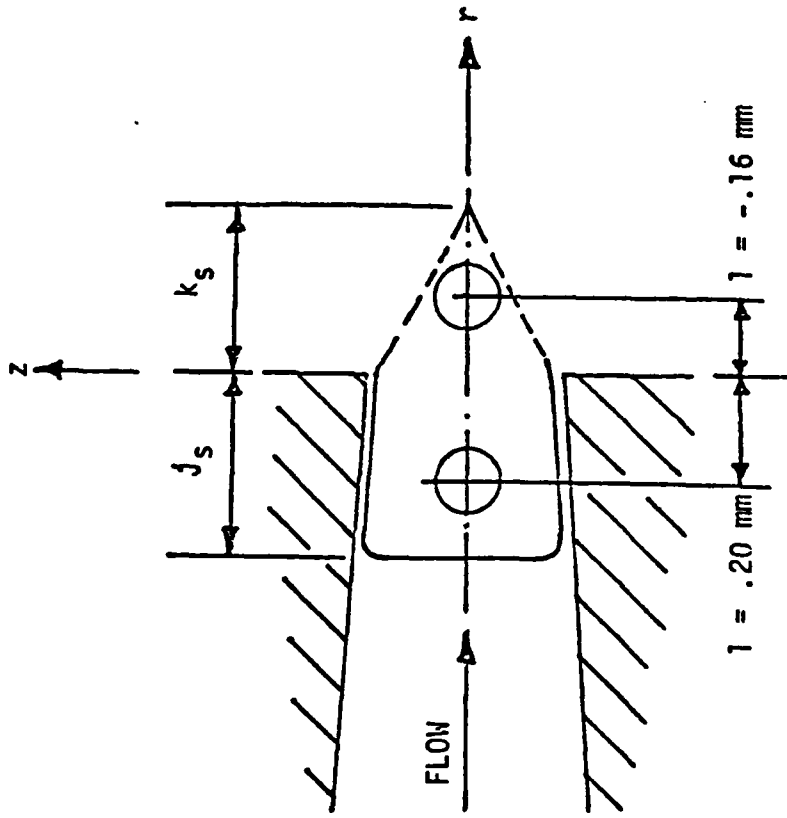Figure 11. Typical motion of a partially trapped light ray in the r and z directions.

Figure 12. Representative shape of the limiting contour of the light well and locations of localized light injection into Venus Machine. Circles indicate area estimated to include 90% of the power of the laser beam. Well shape is representative for the data of figures 8 and 9 for R > 50.